

# MIMO Detection with Spatial Sigma-Delta ADCs: A Variational Bayesian Approach

Toan-Van Nguyen, Sajjad Nassirpour, Italo Atzeni, Antti Tölli, A. Lee Swindlehurst, and Duy H. N. Nguyen

**Abstract**—The spatial Sigma-Delta ( $\Sigma\Delta$ ) architecture can be leveraged to reduce the quantization noise and enhance the effective resolution of few-bit analog-to-digital converters (ADCs) at certain spatial frequencies of interest. Utilizing the variational Bayesian (VB) inference framework, this paper develops novel data detection algorithms tailored for massive multiple-input multiple-output (MIMO) systems with few-bit  $\Sigma\Delta$  ADCs and angular channel models, where uplink signals are confined to a specific angular sector. We start by modeling the corresponding Bayesian networks for the 1<sup>st</sup>- and 2<sup>nd</sup>-order  $\Sigma\Delta$  receivers. Next, we propose an iterative algorithm, referred to as Sigma-Delta variational Bayes (SD-VB), for MIMO detection, offering low-complexity updates through closed-form expressions of the variational densities of the latent variables. Simulation results show that the proposed 2<sup>nd</sup>-order SD-VB algorithm delivers the best symbol error rate (SER) performance while maintaining the same computational complexity as in unquantized systems, matched-filtering VB with conventional quantization, and linear minimum mean-squared error (LMMSE) methods. Moreover, the 1<sup>st</sup>- and 2<sup>nd</sup>-order SD-VB algorithms achieve their lowest SER at an antenna separation of one-fourth wavelength for a fixed number of antenna elements. The effects of the steering angle of the  $\Sigma\Delta$  architecture, the number of ADC resolution bits, and the number of antennas and users are also extensively analyzed.

**Index Terms**—Few-bit quantization, MIMO detection, spatial Sigma-Delta ADCs, variational Bayesian inference.

## I. INTRODUCTION

Beyond-5G wireless systems will require substantial bandwidth in both the millimeter (mmWave) and terahertz (THz) bands to deliver high data throughput [2]. Signals at these frequencies, however, are hindered by low penetration capabilities and high propagation loss, which restrict their practical communication range [3]. Massive multiple-input multiple-output (MIMO) arrays have been used to compensate for the propagation loss while simultaneously achieving high capacity through spatial multiplexing [4]. However, exploiting the full benefits of beamforming and multiplexing in massive MIMO can be challenging due to the need for dedicated high-resolution analog-to-digital converters (ADCs)/digital-to-analog converters (DACs) for each antenna element [5], [6].

Toan-Van Nguyen, Sajjad Nassirpour, and Duy H. N. Nguyen are with the Department of Electrical and Computer Engineering, San Diego State University, San Diego, CA 92182 USA (emails: {nguyen58, snassirpour, duy.nguyen}@sdsu.edu).

Italo Atzeni and Antti Tölli are with the Centre for Wireless Communications, University of Oulu, Finland (emails: {italo.atzeni, antti.tolli}@oulu.fi).

A. Lee Swindlehurst is with the Department of Electrical Engineering and Computer Science, University of California, Irvine, CA, USA (email: swindle@uci.edu).

A portion of this paper has been accepted for presentation at the 2024 Asilomar Conference on Signals, Systems, and Computers, Pacific Grove, CA, USA, Oct. 2024 [1].

This results in high hardware complexity and increased power consumption, especially with larger bandwidths and sampling rates [7]. To address these concerns, the use of low-resolution ADCs with, e.g., 1–3 bits of precision, has emerged as an energy-efficient and low-complexity solution for massive MIMO systems [8]–[10].

Low-resolution ADCs provide low-complexity and low-power designs for massive MIMO systems, but present challenges due to their non-linear nature [11]. The impact of low-resolution ADCs on MIMO systems has been explored, including analyses of the resulting capacity limits and achievable rates [11]–[15]. These studies demonstrate that low-resolution ADCs degrade system performance metrics such as achievable rate and symbol error rate (SER), especially at medium-to-high signal-to-noise ratios (SNRs), but this negative impact can be mitigated by increasing the number of antennas. This observation indicates that massive MIMO can be effectively operated with few-bit ADCs. However, attaining a good tradeoff between the system performance and the number of quantization bits requires advanced signal processing algorithms and architectural innovations tailored for the specific characteristics of the quantized signals [10], [16].

Sigma-Delta ( $\Sigma\Delta$ ) modulation is a well-established method for time-domain signal processing that encodes analog signals into low-bit-depth digital signals at a very high sampling rate. By combining oversampling and noise shaping,  $\Sigma\Delta$  modulation can achieve high resolution despite using low-bit quantizers [17], [18]. In temporal  $\Sigma\Delta$ , oversampling involves sampling a signal at a rate higher than the Nyquist rate. A negative feedback loop is employed to quantize the difference between the input signal and the quantized output to effectively shape the quantization noise to higher frequencies [17]. A low-pass filter is then used to remove the high-frequency quantization noise while preserving the desired low-frequency signals [19]. The 1<sup>st</sup>-order temporal  $\Sigma\Delta$  approach is widely favored in data-driven applications that demand high precision and low noise, such as audio recording, medical imaging and diagnostics, industrial sensor systems, as well as mobile devices used for signal processing [17]. In massive MIMO, spatial  $\Sigma\Delta$  quantization has been used to enhance channel estimation and spectral efficiency [18], [20]. In spatial  $\Sigma\Delta$ , the difference between the input and the quantized output represents the quantization noise at each antenna, which is fed back and compared with the input to an adjacent antenna. This feedback enables more aggressive noise shaping, where the spatial spectrum of the quantization noise is pushed away from the spatial frequencies of interest [21].

### A. Related Works

Communications in the mmWave and THz bands typically require large antenna arrays at the base stations (BS). Here, the implementation of one-bit ADCs for every antenna element can reduce radio-frequency complexity, cost, and power consumption [22], [23]. In [24], a likelihood function learning method for data detection was proposed with one-bit ADCs using an approach based on reinforcement learning. In [16], [25], a support vector machine (SVM)-based channel estimation and data detection method was exploited for one-bit massive MIMO systems, yielding a data detection performance close to that of maximum-likelihood detection. Data detection based on supervised learning was proposed for few-bit MIMO systems in [26], whereas an approach based on deep neural networks was developed in [27]. These learning-based methods necessitate a significant training load, and the neural network must be retrained with new channel realizations [27], thereby increasing the computational complexity. To efficiently balance the performance and complexity for systems with few-bit ADCs, variational Bayes (VB) inference, inspired by machine learning, was proposed for data detection and channel estimation in [10]. The goal of VB is to find an approximation for the true posterior distribution of latent variables given the observed data [28]. VB has also been used in the context of joint channel estimation and data detection in massive MIMO [29] and orthogonal frequency-division multiplexing systems with few-bit ADCs [30]. However, there is no prior work that has considered VB for MIMO detection with  $\Sigma\Delta$  ADCs.

Recently, spatial  $\Sigma\Delta$  ADCs in massive MIMO systems have attracted growing interest in terms of channel estimation [18], [21], performance analysis [18], [20], [31], and precoding design [32]. In [20], the spectral efficiency of 1-bit  $\Sigma\Delta$  massive MIMO was analyzed, revealing that one-bit  $\Sigma\Delta$  scales down the quantization noise power proportionally to the square of the spatial oversampling rate. Spatial few-bit  $\Sigma\Delta$  ADCs have also been used in massive MIMO to shape the quantization noise away from users in certain angular sectors for improved channel estimation [18]. In [31], a parallel  $\Sigma\Delta$  ADC was designed for mmWave receivers to achieve high-resolution outputs; however, the bit-error-rate performance of this design with 3-bit quantization was not significantly improved at high SNRs. 1<sup>st</sup>- and 2<sup>nd</sup>-order  $\Sigma\Delta$  quantization was employed for wide-band systems in [33] without considering the angle steering mechanism. A reconfigurable intelligent surface controlled by a single-antenna base station equipped with 1<sup>st</sup>-order  $\Sigma\Delta$  modulation was investigated in [34]. Mutual coupling effects for phase quantization were considered for dense  $\Sigma\Delta$  phased arrays in [35].

### B. Motivations and Contributions

A common approach in the aforementioned works on  $\Sigma\Delta$  ADCs is to exploit the Busgang decomposition, which reformulates the nonlinear quantization as a linear function, followed for example by standard linear data detection and channel estimation methods [11], [18], [32]. However, the Busgang decomposition is based on the assumption of Gaussian signals, which may not hold at high SNR when the chan-

nels are specular and there are few users. The VB method has been proposed as an alternative to effectively address the nonlinear quantization operation. It is considered superior to linear methods, bilinear generalized approximate message passing [29], and other approaches based on deep learning [36]. However, these studies are limited to conventional few-bit ADCs. More importantly, achieving optimal MIMO detection with spatial  $\Sigma\Delta$  ADCs under the maximum-a-posteriori (MAP) probability criterion may not be feasible. These observations prompt the development in this paper of novel data detection algorithms based on the VB inference framework for MIMO systems with spatial  $\Sigma\Delta$  ADCs.

The contributions of the paper are summarized as follows:

- We develop 1<sup>st</sup>- and 2<sup>nd</sup>-order Sigma-Delta Variational Bayes (SD-VB) detection algorithms, where few-bit  $\Sigma\Delta$  quantizers are employed in a massive MIMO system. We model the Bayesian network for the  $\Sigma\Delta$  receivers, which reveals insightful dependencies between the observed and latent variables.
- We develop the 1<sup>st</sup>- and 2<sup>nd</sup>-order SD-VB algorithms for the 1<sup>st</sup>- and 2<sup>nd</sup>-order  $\Sigma\Delta$  ADC architectures with efficient updates based on the analysis of the variational densities. We also present an LMMSE detector for MIMO detection with 1<sup>st</sup>-order  $\Sigma\Delta$  quantization. The results show that the 1<sup>st</sup>- and 2<sup>nd</sup>-order SD-VB algorithms have the same computational complexity as the matched-filter quantized VB (MF-QVB) algorithm [10], and significantly lower complexity than the LMMSE detector.
- We demonstrate through simulation results that the 2<sup>nd</sup>-order SD-VB algorithm achieves the lowest SER compared with state-of-the-art detection algorithms such as MF-QVB and LMMSE for certain angular sectors. Moreover, the 1<sup>st</sup>-order SD-VB algorithm is more efficient than 2<sup>nd</sup>-order SD-VB for 1-bit ADCs.

The rest of the paper is organized as follows. Section II introduces the system model as well as the model for few-bit  $\Sigma\Delta$  ADCs. The optimal solution for the LMMSE detector based on the linearized model is derived in Section III. Section IV analyzes and discusses the VB framework for detection in a 1<sup>st</sup>-order  $\Sigma\Delta$  MIMO system. Then, Section V extends the VB framework to the 2<sup>nd</sup>-order  $\Sigma\Delta$  case. Numerical results are provided in Section VI and Section VII concludes the paper.

*Notation:* Boldface lowercase and boldface uppercase variables denote vectors and matrices, respectively. The  $i$ -th element of a vector  $\mathbf{x}$  is represented by  $[\mathbf{x}]_i$  and the  $(i, j)$ -th element of a matrix  $\mathbf{X}$  is denoted by  $[\mathbf{X}]_{i,j}$ . The symbols  $\mathbb{C}$  and  $\mathbb{R}$  stand for the sets of complex and real numbers, respectively. The  $L_2$ -norm and the absolute value are indicated by  $\|\cdot\|$  and  $|\cdot|$ , respectively. Real and imaginary parts are denoted by  $\Re\{\cdot\}$  and  $\Im\{\cdot\}$ , respectively, with  $j = \sqrt{-1}$ . A circularly symmetric complex Gaussian (CSCG) distribution with mean  $\boldsymbol{\eta}$  and covariance matrix  $\mathbf{Z}$  is indicated by  $\mathcal{CN}(\boldsymbol{\eta}, \mathbf{Z})$ . The identity matrix is denoted by  $\mathbf{I}$ , the trace operator by  $\text{Tr}(\cdot)$ , and the expectation operator by  $\mathbb{E}\{\cdot\}$ . The transpose, complex conjugate, and complex conjugate transpose operators are denoted by  $(\cdot)^T$ ,  $(\cdot)^*$ , and  $(\cdot)^H$ , respectively.

## II. SYSTEM MODEL

### A. Channel Model

We consider an uplink MIMO system consisting of  $K$  single-antenna users and a BS equipped with a uniform linear array (ULA) of  $N$  antennas. The received signal  $\mathbf{x}$  at the BS before quantization can be expressed as

$$\mathbf{x} = \mathbf{H}\mathbf{s} + \mathbf{n}, \quad (1)$$

where  $\mathbf{H} = [\mathbf{h}_1, \dots, \mathbf{h}_N]^T \in \mathbb{C}^{N \times K}$  is the uplink channel matrix, with  $\mathbf{h}_i \in \mathbb{C}^{K \times 1}$  denoting the channel vector from the  $K$  users to the  $i$ -th antenna at the BS,  $\mathbf{s} = [s_1, \dots, s_K]^T \in \mathbb{C}^{K \times 1}$  is the uplink data symbol vector, and  $\mathbf{n} \sim \mathcal{CN}(\mathbf{0}, N_0 \mathbf{I}_N)$  represents additive Gaussian noise at the BS with variance  $N_0$ . We assume that the channel  $\mathbf{H}$  is known at the BS. The symbol  $s_k$  transmitted from user- $k$  is drawn from a complex-valued discrete constellation  $\mathcal{S}$ , e.g., quadrature amplitude modulation (QAM) or phase-shift keying (PSK), with  $\mathbb{E}[s_k] = 0$  and normalized such that  $\mathbb{E}[|s_k|^2] = 1$ . The prior distribution of  $s_k$  can be expressed as

$$p(s_k) = \sum_{a \in \mathcal{S}} p_a \delta(s_k - a), \quad (2)$$

where  $p_a$  is the known prior probability of the constellation point  $a$  and  $\delta(s_k - a)$  indicates the point mass function at  $a$ .

We assume a geometric channel model typical of mmWave communications systems in which the channel for each user is composed of a linear combination of  $L$  propagation paths [3], [37], i.e.,

$$\bar{\mathbf{h}}_k = \sqrt{\frac{\beta_k}{L}} \mathbf{A}_k \mathbf{g}_k, \quad (3)$$

where  $\bar{\mathbf{h}}_k$  is the  $k$ th column of  $\mathbf{H}$  and the uplink channel from user- $k$ , the columns of  $\mathbf{A}_k \in \mathbb{C}^{N \times L}$  represent the array response for  $L$  propagation paths,  $\mathbf{g}_k \sim \mathcal{CN}(\mathbf{0}, \mathbf{I}_L)$  represents the small-scale fading, and  $\beta_k$  models the geometric attenuation and slow fading. We assume that  $\mathbf{A}_k$  is a full rank matrix whose  $\ell$ -th column is the array steering vector corresponding to the angle of arrival (AoA)  $\theta_{k\ell}$  of the  $\ell$ -th path, as given by

$$\mathbf{a}(\theta_{k\ell}) = [1, e^{-j2\pi \frac{d}{\lambda} \sin \theta_{k\ell}}, \dots, e^{-j(N-1)2\pi \frac{d}{\lambda} \sin \theta_{k\ell}}]^T, \quad (4)$$

where  $d$  is the inter-antenna spacing of the ULA and  $\lambda$  denotes the wavelength. For simplicity, we denote  $\omega_{k\ell} = 2\pi \frac{d}{\lambda} \sin \theta_{k\ell}$  as the spatial frequency of the  $\ell$ -th path from user- $k$ . We assume that the AoAs for all users are situated within a specific angular sector  $\mathcal{S}_{\theta_0} \triangleq [\theta_0 - \Theta/2, \theta_0 + \Theta/2]$ , where  $\theta_0$  is the center angle of the sector and  $\Theta$  is the azimuth angular spread. This constraint frequently arises in practice because cell sectoring limits service to users within a specific angular sector of the BS coverage. Additionally, the high frequency and directional nature of mmWave signals produce narrow beam patterns and substantial attenuation of distant reflections, making nearby reflections of users more dominant and resulting in narrower angular spreads for users.

The received analog signals are then quantized using few-bit ADCs. The mathematical models for both conventional and

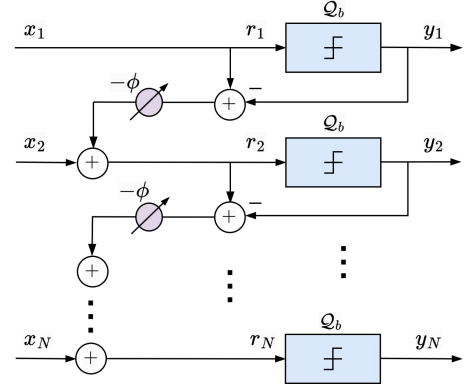


Fig. 1: Illustration of the spatial 1<sup>st</sup>-order  $\Sigma\Delta$  architecture at an  $N$ -antenna receiver.

$\Sigma\Delta$  quantizers in these few-bit ADCs will be detailed in the following subsection.

### B. MIMO Receiver with Few-Bit ADCs

1) *Few-Bit ADCs with Conventional Quantizers*: The received analog signal at each BS antenna is sampled to produce a discrete-time signal, which is then quantized by a pair of  $b$ -bit ADCs to one of a set of discrete quantized levels. Thus, the quantized signal  $\mathbf{y} = \mathcal{Q}_b(\mathbf{x})$  can be modeled as

$$\Re\{\mathbf{y}\} = \mathcal{Q}_b(\Re\{\mathbf{x}\}), \quad \Im\{\mathbf{y}\} = \mathcal{Q}_b(\Im\{\mathbf{x}\}), \quad (5)$$

where  $\mathcal{Q}_b(\cdot)$  denotes the  $b$ -bit ADC operation applied element-wise to its vector argument. The uniform quantizer  $\mathcal{Q}_b(\cdot)$  performs  $b$ -bit scalar quantization which produces  $2^b - 1$  quantized output levels belonging to the set  $\{d_1, \dots, d_{2^b-1}\}$ . Without loss of generality, we assume  $-\infty = d_0 < d_1 \dots < d_{2^b-1} < d_{2^b} = +\infty$ . The quantization thresholds are given by [10]

$$d_m = (-2^{b-1} + m)\Lambda, \quad \forall m \in \mathcal{M} = 1, \dots, 2^b - 1, \quad (6)$$

where  $\Lambda$  denotes the quantization step size of  $\mathcal{Q}_b(\cdot)$ . The quantized output  $q_i$  at the  $i$ -th antenna of the BS is defined as

$$q_i = \mathcal{Q}_b(x_i) = \begin{cases} d_m - \frac{\Lambda}{2}, & \text{if } x_i \in (d_{m-1}, d_m), \\ (2^b - 1) \frac{\Lambda}{2}, & \text{if } x_i \in (d_{2^b-1}, d_{2^b}). \end{cases} \quad (7)$$

We also define by  $q_i^{\text{up}}$  and  $q_i^{\text{low}}$  the upper and lower thresholds of the quantization bin to which  $q_i$  belongs.

2) *Few-Bit ADCs with Sigma-Delta Quantizers*: The  $\Sigma\Delta$  quantization process is illustrated in Fig. 1, where a few-bit quantizer is used in each quantization block. The pre-quantized signal at stage  $i$ , denoted by  $r_i$ , which consists of the unquantized received signal  $x_i$  and the difference between the input and output of the previous quantizer, can be represented as [18], [20]

$$r_i = x_i + e^{-j\phi}(r_{i-1} - y_{i-1}), \quad \forall i = 1, \dots, N, \quad (8)$$

where  $x_i \triangleq \mathbf{h}_i^T \mathbf{s} + n_i$  is the unquantized received signal at antenna  $i$ ,  $r_0$  and  $y_0$  are set to 0, and  $\phi$  denotes a phase shift applied to the signal between two adjacent antennas. After

quantization, the observation at the  $i$ -th antenna element can be expressed as

$$y_i = \mathcal{Q}_b(r_i). \quad (9)$$

Using spatial oversampling with antenna elements spaced closer than one-half wavelength, and feedback of the quantization error between adjacent antennas, the  $\Sigma\Delta$  architecture shapes the quantization noise to higher spatial frequencies, thereby significantly reducing it for signals arriving from angles closer to the broadside of the ULA (when  $\phi = 0$ ). However, there is a practical limit to using spatial oversampling due to the physical dimensions of the antennas and mutual coupling. For this reason, the  $\Sigma\Delta$  architecture is best suited for scenarios where two conditions are met: the array incorporates spatial oversampling and the users of interest are confined within a specific angular sector [18].

In the following, we present a linearized model for spatial 1<sup>st</sup>-order  $\Sigma\Delta$  ADCs and the corresponding linear minimum mean squared error (LMMSE) receiver to estimate  $\mathbf{s}$ . Subsequent developments will include the design of efficient VB-based MIMO detection algorithms for 1<sup>st</sup>- and 2<sup>nd</sup>-order  $\Sigma\Delta$  ADCs.

### III. LINEAR DETECTION WITH SPATIAL $\Sigma\Delta$ QUANTIZED OBSERVATIONS

Using the Bussgang decomposition [38], the output of the  $\Sigma\Delta$  array in (9) in vector form is linearized as [20, Eq. (16)]:

$$\mathbf{y} = \mathbf{H}\mathbf{x} + \mathbf{U}^{-1}\mathbf{q}, \quad (10)$$

where  $\mathbf{q} = [q_1, \dots, q_N]^T$  represents the effective quantization noise, and  $\mathbf{U}$  is defined as

$$\mathbf{U} = \begin{bmatrix} 1 & 0 & \dots & 0 & 0 \\ e^{-j\phi} & 1 & \dots & 0 & 0 \\ e^{-j2\phi} & e^{-j\phi} & \dots & 0 & 0 \\ \vdots & \vdots & \ddots & \ddots & \vdots \\ e^{-j(N-1)\phi} & e^{-j(N-2)\phi} & \dots & e^{-j\phi} & 1 \end{bmatrix}. \quad (11)$$

For the special case of one-bit  $\Sigma\Delta$  quantization, the variance of  $q_i$  is given by [20, Eq. (33)]

$$\tau_{q_i} = \left(\frac{\pi}{2} - 1\right) \frac{1 - (\pi/2 - 1)^i}{2 - \pi/2} p_s, \quad (12)$$

where  $p_s$  is the power of the received signal at the  $i$ -th antenna.

Based on the linearized model in (10), an LMMSE receiver  $\mathbf{W}_{\text{LMMSE}}$  that minimizes the mean squared error  $\mathbb{E}[\|\mathbf{s} - \mathbf{W}\mathbf{y}\|^2]$  in estimating  $\mathbf{s}$  can be expressed as

$$\mathbf{W}_{\text{LMMSE}} = \Sigma_{\mathbf{s}}\mathbf{H}^H(\mathbf{H}\Sigma_{\mathbf{s}}\mathbf{H}^H + N_0\mathbf{I}_N + \mathbf{U}^{-1}\Sigma_{\mathbf{q}}\mathbf{U}^{-H})^{-1}, \quad (13)$$

where  $\Sigma_{\mathbf{s}}$  and  $\Sigma_{\mathbf{q}} = \text{diag}(\tau_{q_1}, \dots, \tau_{q_N})$  are the covariance matrices of  $\mathbf{s}$  and  $\mathbf{q}$ , respectively. As mentioned earlier, the accuracy of the Bussgang decomposition depends on the Gaussianity of the input to the quantization non-linearity, which does not always hold, particularly when the input symbol is discrete. To overcome this challenge, in the next section, we introduce an alternative MIMO detection approach based on VB inference to handle the nonlinear  $\Sigma\Delta$  receiver architecture.

## IV. VARIATIONAL BAYES FOR FEW-BIT 1<sup>st</sup>-ORDER $\Sigma\Delta$ MIMO DETECTION

In this section, we first provide background on VB inference and then develop a new data detection method based on the VB framework in few-bit  $\Sigma\Delta$  MIMO systems with known channel  $\mathbf{H}$ .

### A. Background on VB Inference

We denote the set of all observed variables as  $\mathbf{y}$  and the set of  $V$  latent variables as  $\mathbf{x}$ . To find a Bayes estimate of  $\mathbf{x}$ , one would need to determine the posterior distribution  $p(\mathbf{x}|\mathbf{y})$ , which is often computationally intractable. To overcome this challenge, the VB method aims to find a distribution  $q(\mathbf{x})$  characterized by variational parameters within a predefined family  $\mathcal{Q}$  of densities, such that  $q(\mathbf{x})$  closely approximates  $p(\mathbf{x}|\mathbf{y})$ . To this end, VB defines an optimization problem leveraging the Kullback-Leibler (KL) divergence from  $q(\mathbf{x})$  to  $p(\mathbf{x}|\mathbf{y})$ :

$$\begin{aligned} q^*(\mathbf{x}) &= \arg \min_{q(\mathbf{x}) \in \mathcal{Q}} \text{KL}(q(\mathbf{x})\|p(\mathbf{x}|\mathbf{y})), \\ &= \arg \min_{q(\mathbf{x}) \in \mathcal{Q}} \left\{ \mathbb{E}_{q(\mathbf{x})} [\ln q(\mathbf{x})] - \mathbb{E}_{q(\mathbf{x})} [\ln p(\mathbf{x}|\mathbf{y})] \right\}, \end{aligned} \quad (14)$$

where  $q^*(\mathbf{x})$  denotes the optimal variational distribution. The VB method assumes that  $q(\mathbf{x})$  is drawn from the mean-field variational family [39], such that

$$q(\mathbf{x}) = \prod_{i=1}^V q_i(x_i), \quad (15)$$

where the latent variables are mutually independent, with each being governed by a distinct factor in the variational density. The optimal value of  $q_i(x_i)$  is obtained as [39, Chapter 10]

$$q_i^*(x_i) \propto \exp \left\{ \langle \ln p(\mathbf{y}, \mathbf{x}) \rangle \right\}, \quad (16)$$

where  $\langle \cdot \rangle$  is the expectation w.r.t. all latent variables except  $x_i$ , utilizing the currently fixed variational density  $q_{-i}(\mathbf{x}_{-i}) = \prod_{j=1, j \neq i}^V q_j(x_j)$ . To optimize (14), we use the Coordinate Ascent Variational Inference algorithm, which is an iterative method that ensures convergence to at least a locally optimal solution [40].

### B. VB Inference for Few-bit $\Sigma\Delta$ MIMO Detection

Considering the input-output relationship of the 1<sup>st</sup>-order  $\Sigma\Delta$  quantizer in (8), the conditional distributions between the observed quantized signal  $y_i$  and latent variables, i.e.,  $r_i$ ,  $x_i$ ,  $\mathbf{s}$ , are given by  $p(r_i|r_{i-1}, y_{i-1}, \mathbf{s}; \mathbf{H}, N_0) = \mathcal{CN}(r_i; \mathbf{h}_i^T \mathbf{s} + e^{-j\phi}(r_{i-1} - y_{i-1}), N_0)$  and  $p(y_i|r_i) = \mathbb{1}(r_i \in [y_i^{\text{low}}, y_i^{\text{up}}])$ , where  $\mathbb{1}$  is the indicator function which equals one if the argument holds, or zero otherwise. The optimal MAP detector  $\hat{\mathbf{s}}_{\text{MAP}} = \arg \max_{\mathbf{s} \in \mathcal{S}^K} p(\mathbf{y}, \mathbf{s}; \mathbf{H}, N_0)$  with spatial  $\Sigma\Delta$  ADCs can be written as

$$\begin{aligned} \hat{\mathbf{s}}_{\text{MAP}} &= \arg \max_{\mathbf{s} \in \mathcal{S}^K} \int p(\mathbf{y}, \mathbf{r}, \mathbf{s}; \mathbf{H}, N_0) d\mathbf{r} \\ &= \arg \max_{\mathbf{s} \in \mathcal{S}^K} p(\mathbf{s}) \int \prod_{i=1}^N p(y_i|r_i) p(r_i|r_{i-1}, y_{i-1}, \mathbf{s}; \mathbf{H}, N_0) d\mathbf{r}. \end{aligned} \quad (17)$$

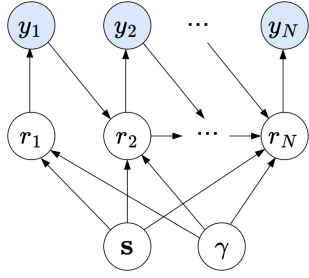


Fig. 2: The Bayesian network for the 1<sup>st</sup>-order  $\Sigma\Delta$  receiver.

This integral is intractable to evaluate in closed-form due to the high dimensional integration and the intricate correlation between  $\mathbf{r}$  and  $\mathbf{s}$ . This challenge motivates us to explore a novel VB inference method to solve the data detection problem with  $\Sigma\Delta$  arrays.

We consider the residual interference-plus-noise as an unknown parameter  $N_0^{\text{post}}$ , which must be estimated using the VB method. The dependency between random variables under spatial  $\Sigma\Delta$  processing can be graphically modeled through the Bayesian network in Fig. 2, where  $\gamma \triangleq 1/N_0^{\text{post}}$  denotes the precision that is floated as an unknown random variable and the arrows indicate the conditional probability between variables. The main goal is to infer the distribution of data  $\mathbf{s}$  given the observation  $\mathbf{y}$ . To accomplish this, we employ the mean-field variational distribution  $q(\mathbf{s}, \mathbf{r}, \gamma)$ , such that

$$p(\mathbf{s}, \mathbf{r}, \gamma | \mathbf{y}; \mathbf{H}) \approx q(\mathbf{s}, \mathbf{r}, \gamma) = \prod_{k=1}^K q(s_k) \prod_{i=1}^N q(r_i) q(\gamma). \quad (18)$$

According to (16), to obtain the optimal solution of the variational densities in (18), we need the joint distribution  $p(\mathbf{y}, \mathbf{r}, \mathbf{s}, \gamma; \mathbf{H})$  which can be factorized as

$$p(\mathbf{y}, \mathbf{r}, \mathbf{s}, \gamma; \mathbf{H}) = p(\mathbf{s}) p(\gamma) \times \prod_{i=1}^N p(y_i | r_i) p(r_i | r_{i-1}, y_{i-1}, \mathbf{s}, \gamma; \mathbf{H}), \quad (19)$$

where

$$p(r_i | r_{i-1}, y_{i-1}, \mathbf{s}, \gamma; \mathbf{H}) = \mathcal{CN}(r_i; \mathbf{h}_i^T \mathbf{s} + e^{-j\phi}(r_{i-1} - y_{i-1}), \gamma^{-1}). \quad (20)$$

To this end, we present the update process for each latent variable through the derived closed-form expression of each variational density.

1) *Updating  $r_i$* : For  $i = 1, \dots, N-1$ , the variational distribution  $q(r_i)$  can be obtained by taking the expectation

of the conditional in (19) w.r.t.  $q(\mathbf{s}, \gamma)$  as

$$\begin{aligned} q(r_i) &\propto \exp \left\{ \left\langle \ln p(y_i | r_i) + \ln p(r_{i+1} | r_i, y_i, \mathbf{s}, \gamma; \mathbf{H}) \right. \right. \\ &\quad \left. \left. + \ln p(r_i | r_{i-1}, y_{i-1}, \mathbf{s}, \gamma; \mathbf{H}) \right\rangle \right\} \\ &\propto p(y_i | r_i) \exp \left\{ - \langle \gamma | r_i - \mathbf{h}_i^T \mathbf{s} - e^{-j\phi}(r_{i-1} - y_{i-1})|^2 \rangle \right. \\ &\quad \left. - \langle \gamma | r_{i+1} - \mathbf{h}_{i+1}^T \mathbf{s} - e^{-j\phi}(r_i - y_i)|^2 \rangle \right\} \\ &\propto p(y_i | r_i) \exp \left\{ - \langle \gamma \rangle (|r_i - a_i|^2 + |r_i - b_i|^2) \right\} \\ &\propto \mathbb{1}(r_i \in [y_i^{\text{low}}, y_i^{\text{up}}]) \mathcal{CN}(r_i; (a_i + b_i)/2, 1/(2\langle \gamma \rangle)), \end{aligned} \quad (21)$$

where  $a_i \triangleq \mathbf{h}_i^T \langle \mathbf{s} \rangle + e^{-j\phi}(\langle r_{i-1} \rangle - y_{i-1})$  and  $b_i \triangleq y_i + e^{j\phi} \langle r_{i+1} \rangle - e^{j\phi} \mathbf{h}_{i+1}^T \langle \mathbf{s} \rangle$ .

Defining  $v_i \triangleq (a_i + b_i)/2$ , we see that the variational distribution  $q(r_i)$  in (21) is a truncated complex Gaussian distribution obtained by pruning the distribution  $\mathcal{CN}(v_i, 1/(2\langle \gamma \rangle))$  onto the interval  $[y_i^{\text{low}}, y_i^{\text{up}}]$ . In Appendix A we show that the mean and variance of the resulting distribution are given by  $\langle r_i \rangle = F_r(v_i, 2\langle \gamma \rangle, y_i^{\text{low}}, y_i^{\text{up}})$  and  $\tau_{r_i} = G_r(v_i, 2\langle \gamma \rangle, y_i^{\text{low}}, y_i^{\text{up}})$ , respectively.

For  $i = N$ , while the factor  $p(r_{N+1} | r_N, y_N, \mathbf{s}, \gamma; \mathbf{H})$  does not exist, the variational distribution  $q(r_N)$  can be computed similarly to (21) and is given by

$$q(r_N) \propto \mathbb{1}(r_N \in [y_N^{\text{low}}, y_N^{\text{up}}]) \mathcal{CN}(r_N; a_N, 1/\langle \gamma \rangle). \quad (22)$$

2) *Updating  $s_k$* : The variational distribution  $q(s_k)$  is obtained by taking the expectation of the conditional in (19) w.r.t.  $q(\mathbf{r}, \gamma)$ :

$$\begin{aligned} q(s_k) &\propto \exp \left\{ \left\langle \ln p(s_k) + \sum_{i=1}^N \ln p(r_i | r_{i-1}, y_{i-1}, \mathbf{s}, \gamma; \mathbf{H}) \right\rangle \right\} \\ &\propto p(s_k) \exp \left\{ - \langle \gamma \rangle \sum_{i=1}^N \left\langle |r_i - \mathbf{h}_i^T \mathbf{s} \right. \right. \\ &\quad \left. \left. - e^{-j\phi}(r_{i-1} - y_{i-1})|^2 \right\rangle \right\}. \end{aligned} \quad (23)$$

Expanding  $\mathbf{h}_i^T \mathbf{s} = h_{i,k} s_k + \sum_{j \neq k} h_{i,j} s_j$  leads to

$$\begin{aligned} q(s_k) &\propto p(s_k) \exp \left\{ - \langle \gamma \rangle \sum_{i=1}^N \left| \langle r_i \rangle - \sum_{j \neq k} h_{i,j} \langle s_j \rangle \right. \right. \\ &\quad \left. \left. - e^{-j\phi}(\langle r_{i-1} \rangle - y_{i-1}) - h_{i,k} s_k \right|^2 \right\} \\ &\propto p(s_k) \exp \left\{ - \langle \gamma \rangle \sum_{i=1}^N |z_{i,k} - h_{i,k} s_k|^2 \right\} \\ &\propto p(s_k) \prod_{i=1}^N \mathcal{CN}(z_{i,k}; h_{i,k} s_k, \langle \gamma \rangle^{-1}), \end{aligned} \quad (24)$$

where

$$\begin{aligned} z_{i,k} &= \langle r_i \rangle - e^{-j\phi}(\langle r_{i-1} \rangle - y_{i-1}) - \sum_{j \neq i} h_{i,j} \langle s_j \rangle \\ &= \langle r_i \rangle - e^{-j\phi}(\langle r_{i-1} \rangle - y_{i-1}) - \mathbf{h}_i^T \langle \mathbf{s} \rangle + h_{i,k} \langle s_k \rangle, \end{aligned} \quad (25)$$

using the current estimate  $\langle s_k \rangle$  for all  $k = 1, \dots, K$ . Inter-

estingly, the variational distribution  $q(s_k)$  is equivalent to the posterior distribution  $p(s_k|\mathbf{z}_k, \langle\gamma\rangle; \mathbf{h}_k)$  of  $s_k$  in a single-input multiple-output (SIMO) system:

$$\mathbf{z}_k = \mathbf{h}_k s_k + \mathcal{CN}(\mathbf{0}, \langle\gamma\rangle^{-1} \mathbf{I}_N) \quad (26)$$

where  $\mathbf{z}_k = [z_{1,k}, \dots, z_{N,k}]^T$ . The variational mean and variance of  $s_k$  can be expressed as  $\langle s_k \rangle = \mathbf{F}_s(\mathbf{z}_k, \mathbf{h}_k, \langle\gamma\rangle)$  and  $\tau_{s_k} = \mathbf{G}_s(\mathbf{z}_k, \mathbf{h}_k, \langle\gamma\rangle)$ , respectively, as shown in Appendix B.

3) *Updating  $\gamma$* : We assume a conjugate prior Gamma distribution  $\text{Gamma}(\alpha, \beta)$  for the precision  $\gamma$ , for given shape and rate parameters  $\alpha$  and  $\beta$ , respectively. The variational distribution  $q(\gamma)$  is obtained by taking the expectation of the conditional distribution in (19) w.r.t.  $q(\mathbf{s}, \mathbf{r})$ :

$$\begin{aligned} q(\gamma) &\propto \exp \left\{ \left\langle \sum_{i=1}^N \ln p(r_i | r_{i-1}, y_{i-1}, \mathbf{s}, \gamma; \mathbf{H}) + \ln p(\gamma) \right\rangle \right\} \\ &\propto \exp \left\{ -\gamma \sum_{i=1}^N \langle |r_i - \mathbf{h}_i^T \mathbf{s} - e^{-j\phi}(r_{i-1} - y_{i-1})|^2 \rangle \right. \\ &\quad \left. + N \ln \gamma + (\alpha - 1) \ln \gamma - \beta \gamma \right\} \\ &\propto \exp \left\{ -\gamma \sum_{i=1}^N (\langle |r_i - \mathbf{h}_i^T \mathbf{s}|^2 \rangle + \langle |r_{i-1} - y_{i-1}|^2 \rangle \right. \\ &\quad \left. - 2 \Re \{ \langle (r_i - \mathbf{h}_i^T \mathbf{s})^* (r_{i-1} - y_{i-1}) e^{-j\phi} \rangle \}) \right. \\ &\quad \left. + (N + \alpha - 1) \ln \gamma - \beta \gamma \right\}. \quad (27) \end{aligned}$$

Using the expansion  $\langle |r_i - \mathbf{h}_i^T \mathbf{s}|^2 \rangle = \langle |r_i| - \mathbf{h}_i^T \langle \mathbf{s} \rangle \rangle^2 + \tau_{r_i} + \mathbf{h}_i^T \Sigma_s \mathbf{h}_i$ , we arrive at

$$\begin{aligned} q(\gamma) &\propto \exp \left\{ -\gamma \sum_{i=1}^N \left[ \langle |r_i| - \mathbf{h}_i^T \langle \mathbf{s} \rangle - \langle (r_{i-1}) - y_{i-1} \rangle e^{-j\phi} \right]^2 \right. \\ &\quad \left. + \tau_{r_i} + \mathbf{h}_i^H \Sigma_s \mathbf{h}_i + \tau_{r_{i-1}} \right] + (N + \alpha - 1) \ln \gamma - \beta \gamma \left\} \\ &\propto \exp \left\{ -\gamma \sum_{i=1}^N \left[ |u_i|^2 + \tau_{r_i} + \mathbf{h}_i^H \Sigma_s \mathbf{h}_i + \tau_{r_{i-1}} \right] \right. \\ &\quad \left. + (N + \alpha - 1) \ln \gamma - \beta \gamma \right\} \\ &\propto \exp \left\{ -\gamma \left[ \beta + \|\mathbf{u}\|^2 + 2\text{Tr}\{\Sigma_r\} - \tau_{r_N} \right. \right. \\ &\quad \left. \left. + \text{Tr}\{\mathbf{H}\Sigma_s\mathbf{H}^H\} \right] + (N + \alpha - 1) \ln \gamma \right\}, \quad (28) \end{aligned}$$

where  $u_i \triangleq \langle r_i \rangle - \mathbf{h}_i^T \langle \mathbf{s} \rangle - e^{-j\phi}(\langle r_{i-1} \rangle - y_{i-1})$ ,  $\mathbf{u} = [u_1, \dots, u_N]^T$  and  $\Sigma_r = \text{diag}(\tau_{r_1}, \dots, \tau_{r_N})$  is the covariance matrix of  $\mathbf{r}$ . Here,  $u_i$  denotes the residual term at receive antenna  $i$ , which would equal the noise term  $n_i$  if  $r_i, r_{i-1}$ , and  $\mathbf{s}$  were perfectly known.

The variational distribution  $q(\gamma)$  is Gamma with mean

$$\langle \gamma \rangle = \frac{N + \alpha}{\beta + \|\mathbf{u}\|^2 + 2\text{Tr}\{\Sigma_r\} - \tau_{r_N} + \text{Tr}\{\mathbf{H}\Sigma_s\mathbf{H}^H\}}. \quad (29)$$

The proposed VB method for MIMO detection with 1<sup>st</sup>-order  $\Sigma\Delta$  quantization is summarized in Algorithm 1, where the parameter  $\epsilon$  is the numerator of  $\hat{\gamma}$  in the variational distributions of (21) and (22) for updating  $r_i$  and  $r_N$ , respectively.

---

### Algorithm 1 – VB Algorithm for MIMO Detection with 1<sup>st</sup>-Order $\Sigma\Delta$ Quantization

---

```

1: Input:  $\mathbf{y}, \mathbf{H}$ 
2: Output:  $\hat{\mathbf{s}}$ 
3: Initialize  $\hat{r}_i^1 = y_i^1, \tau_{r_i}^1 = 0, \forall i, \hat{s}_k^1 = 0, \tau_{s_k}^1 = \text{Var}_{p(s_k)}[s_k], \forall k,$ 
    $\mathbf{u} = \hat{\mathbf{r}}^1 - \mathbf{H}\hat{\mathbf{s}}^1.$ 
4: for  $t = 1, 2, \dots$  do
5:    $\hat{\gamma}^t \leftarrow (N + \alpha) / (\beta + \|\mathbf{u}\|^2 + 2\text{Tr}\{\Sigma_r\} - \tau_{r_N}^t + \text{Tr}\{\mathbf{H}\Sigma_s\mathbf{H}^H\})$ 
6:   for  $i = 1, \dots, N$  do
7:     if  $i = N$  then
8:        $v_i^t = \hat{r}_N^t - u_N, \epsilon = 1$ 
9:     else
10:       $v_i^t \leftarrow \hat{r}_i^t - (u_i - e^{j\phi} u_{i+1}) / 2, \epsilon = 2$ 
11:    end if
12:     $\hat{r}_i^{t+1} \leftarrow \mathbf{F}_r(v_i^t, \epsilon \hat{\gamma}^t, y_i^{\text{low}}, y_i^{\text{up}})$ 
13:     $\tau_{r_i}^{t+1} \leftarrow \mathbf{G}_r(v_i^t, \epsilon \hat{\gamma}^t, y_i^{\text{low}}, y_i^{\text{up}})$ 
14:     $u_i \leftarrow u_i - \hat{r}_i^t + \hat{r}_i^{t+1}$ 
15:     $u_{i+1} \leftarrow u_{i+1} + e^{-j\phi}(\hat{r}_i^t - \hat{r}_i^{t+1})$  only for  $i < N$ 
16:  end for
17:  for  $k = 1, \dots, K$  do
18:     $\mathbf{z}_k^t \leftarrow \mathbf{h}_k \hat{s}_k^t + \mathbf{u}$ 
19:     $\hat{s}_k^{t+1} \leftarrow \mathbf{F}_s(\mathbf{z}_k^t, \mathbf{h}_k, \hat{\gamma}^t)$ 
20:     $\tau_{s_k}^{t+1} \leftarrow \mathbf{G}_s(\mathbf{z}_k^t, \mathbf{h}_k, \hat{\gamma}^t)$ 
21:     $\mathbf{u} \leftarrow \mathbf{u} + \mathbf{h}_k (\hat{s}_k^t - \hat{s}_k^{t+1})$ 
22:  end for
23: end for
24:  $\forall k : \hat{s}_k \leftarrow \arg \max_{a \in \mathcal{S}} p_a \mathcal{CN}(\mathbf{z}_k^t; \mathbf{h}_k a, (1/\hat{\gamma}^t) \mathbf{I}_M)$ 

```

---

*Remark 1:* In Algorithm 1, we use  $\hat{r}_i^t, \hat{s}_k^t,$  and  $\hat{\gamma}^t$  to replace  $\langle r_i \rangle, \langle s_k \rangle,$  and  $\langle \gamma \rangle$  at iteration  $t$ , and each iteration includes a round of updating the estimates of  $\mathbf{r}, \mathbf{s},$  and  $\gamma$ . Recalling  $u_i = \langle r_i \rangle - e^{-j\phi}(\langle r_{i-1} \rangle - y_{i-1}) - \mathbf{h}_i^T \langle \mathbf{s} \rangle,$   $a_i = \mathbf{h}_i^T \langle \mathbf{s} \rangle + e^{-j\phi}(\langle r_{i-1} \rangle - y_{i-1})$  and  $b_i = y_i + e^{j\phi} \langle r_{i+1} \rangle - e^{j\phi} \mathbf{h}_{i+1}^T \langle \mathbf{s} \rangle,$   $a_i$  and  $b_i$  can be rewritten as  $a_i = \hat{r}_i^t - u_i$  and  $b_i = \hat{r}_i^t + e^{j\phi} u_{i+1}$  using the current estimates  $\{\hat{r}_i^t\}$  and  $\{\hat{s}_k^t\}$ . Thus, we have

$$v_i^t = \begin{cases} \frac{a_i + b_i}{2} = \hat{r}_i^t - \frac{u_i - e^{j\phi} u_{i+1}}{2}, & \text{for } i = 1, \dots, N-1, \\ a_N = \hat{r}_N^t - u_N, & \text{for } i = N, \end{cases}$$

in step 7 of Algorithm 1.

*Remark 2:* The residual noise term  $\mathbf{u}$ , initialized as  $\mathbf{u} = \hat{\mathbf{r}}^1 - \mathbf{H}\hat{\mathbf{s}}^1,$  is introduced in lines 14, 15, and 21 of Algorithm 1 to reduce the computational complexity. Due to the sequential nature of VB,  $v_i^t$  and  $\mathbf{z}_k^t$  are calculated using the updated values of  $\hat{\mathbf{r}}$  and  $\hat{\mathbf{s}}$ . Instead of computing  $u_i = \langle r_i \rangle - \mathbf{h}_i^T \langle \mathbf{s} \rangle - e^{-j\phi}(\langle r_{i-1} \rangle - y_{i-1})$  for all elements of  $\mathbf{u}$ , incurring a complexity of  $\mathcal{O}(NK)$ , the current value of the residual noise term  $\mathbf{u}$  is used. The update of  $\mathbf{u}$  reflects any update for the estimates of  $\hat{r}_i$  or  $\hat{s}_k$ , and only incurs a complexity of  $\mathcal{O}(N)$ .

## V. EXTENSION TO MIMO DETECTION WITH 2<sup>nd</sup>-ORDER $\Sigma\Delta$ QUANTIZATION

The 2<sup>nd</sup>-order  $\Sigma\Delta$  architecture provides more aggressive noise shaping, further reducing the quantization noise in the desired angular sector compared to the 1<sup>st</sup>-order case [19]. In this section, we develop a VB approach for MIMO detection with 2<sup>nd</sup>-order  $\Sigma\Delta$  quantization based on the approach of the previous section. The 2<sup>nd</sup>-order spatial  $\Sigma\Delta$  architecture is illustrated in Fig. 3. The phase difference applied between

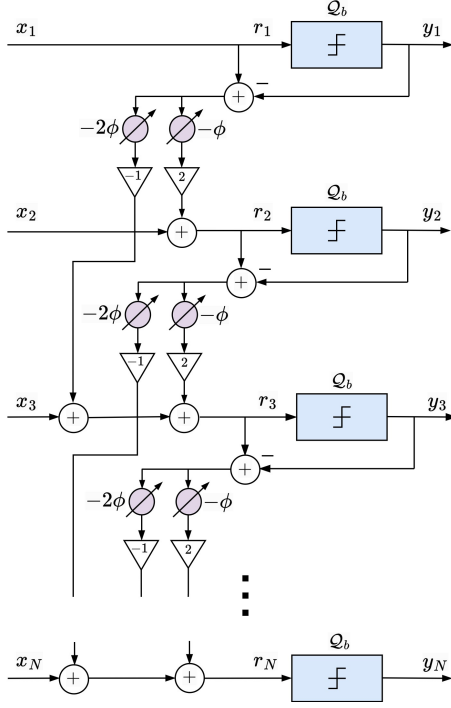


Fig. 3: Illustration of the 2<sup>nd</sup>-order spatial  $\Sigma\Delta$  architecture for a multi-antenna receiver.

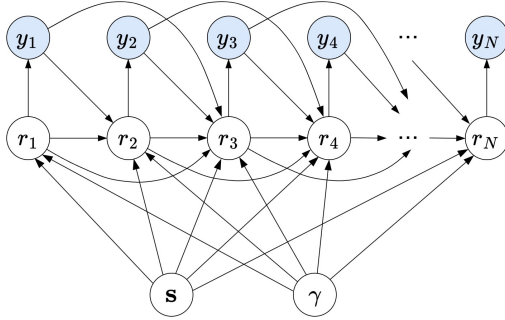


Fig. 4: Bayesian network for the 2<sup>nd</sup>-order  $\Sigma\Delta$  receiver.

antennas  $i$  and  $(i + 1)$  is  $\phi$ , while that between antenna  $i$  and  $(i + 2)$  is  $2\phi$ . The input-output relationship for the 2<sup>nd</sup>-order  $\Sigma\Delta$  approach is given by

$$r_i = x_i + 2e^{-j\phi}(r_{i-1} - y_{i-1}) - e^{-j2\phi}(r_{i-2} - y_{i-2}), \quad (30)$$

$$y_i = Q_b(r_i). \quad (31)$$

#### A. Proposed SD-VB Approach for Data Detection

Based on (30), the dependency between random variables under spatial 2<sup>nd</sup>-order  $\Sigma\Delta$  processing can be illustrated through the graphical Bayesian network model in Fig. 4. The joint distribution  $p(\mathbf{y}, \mathbf{r}, \mathbf{s}, \gamma; \mathbf{H})$  can be factored as

$$p(\mathbf{y}, \mathbf{r}, \mathbf{s}, \gamma; \mathbf{H}) \quad (32)$$

$$= p(\mathbf{s})p(\gamma) \prod_{i=1}^N p(y_i|r_i)p(r_i|r_{i-1}, y_{i-1}, r_{i-2}, y_{i-2}, \mathbf{s}, \gamma; \mathbf{H}),$$

where

$$p(r_i|r_{i-1}, y_{i-1}, r_{i-2}, y_{i-2}, \mathbf{s}, \gamma; \mathbf{H}) = \mathcal{CN}(r_i; \mathbf{h}_i^T \mathbf{s} + 2e^{-j\phi}(r_{i-1} - y_{i-1}) - e^{-j2\phi}(r_{i-2} - y_{i-2}), 1/\gamma). \quad (33)$$

The mean-field VB inference method aims to optimize the variational distribution  $q(\mathbf{s}, \mathbf{r}, \gamma)$  such that

$$p(\mathbf{s}, \mathbf{r}, \gamma; \mathbf{y}; \mathbf{H}) \approx q(\mathbf{s}, \mathbf{r}, \gamma) = \prod_{k=1}^K q(s_k) \prod_{i=1}^N q(r_i)q(\gamma). \quad (34)$$

1) *Updating  $r_i$* : For  $i = 1, \dots, N - 2$ , the variational distribution  $q(r_i)$  can be obtained by taking the expectation of the conditional in (32) w.r.t.  $q(\mathbf{s}, \gamma)$  as

$$q(r_i) \propto \exp \left\{ \left\langle \ln p(r_i|r_{i-1}, y_{i-1}, r_{i-2}, y_{i-2}, \mathbf{s}, \gamma; \mathbf{H}) + \ln p(y_i|r_i) + \ln p(r_{i+1}|r_i, y_i, r_{i-1}, y_{i-1}, \mathbf{s}, \gamma; \mathbf{H}) + \ln p(r_{i+2}|r_{i+1}, y_{i+1}, r_i, y_i, \mathbf{s}, \gamma; \mathbf{H}) \right\rangle \right\}, \quad (35)$$

which is expanded as in (36) on the next page, where

$$\begin{aligned} c_i &\triangleq \mathbf{h}_i^T \langle \mathbf{s} \rangle + 2e^{-j\phi}(\langle r_{i-1} \rangle - y_{i-1}) - e^{-j2\phi}(\langle r_{i-2} \rangle - y_{i-2}), \\ d_i &\triangleq 2y_i + e^{j\phi} \langle r_{i+1} \rangle - e^{j\phi} \mathbf{h}_{i+1}^T \langle \mathbf{s} \rangle + e^{-j\phi}(\langle r_{i-1} \rangle - y_{i-1}), \\ f_i &\triangleq y_i - e^{j2\phi} \langle r_{i+2} \rangle + e^{j2\phi} \mathbf{h}_{i+2}^T \langle \mathbf{s} \rangle + 2e^{j\phi}(\langle r_{i+1} \rangle - y_{i+1}). \end{aligned}$$

Similarly, we can obtain the variational distribution  $q(r_{N-1})$  as

$$q(r_{N-1}) \propto \mathbb{1}(r_{N-1} \in [y_{N-1}^{\text{low}}, y_{N-1}^{\text{up}}]) \times \mathcal{CN}(r_{N-1}; (c_{N-1} + 2d_{N-1})/5, 1/(5\langle \gamma \rangle)), \quad (37)$$

and  $q(r_N)$  as

$$q(r_N) \propto \mathbb{1}(r_N \in [y_N^{\text{low}}, y_N^{\text{up}}]) \mathcal{CN}(r_N; c_N, 1/\langle \gamma \rangle). \quad (38)$$

Defining the residual term  $u_i$  as

$$u_i = \langle r_i \rangle - \mathbf{h}_i^T \langle \mathbf{s} \rangle - 2e^{-j\phi}(\langle r_{i-1} \rangle - y_{i-1}) + e^{-j2\phi}(\langle r_{i-2} \rangle - y_{i-2}), \quad (39)$$

we have  $c_i = \langle r_i \rangle - u_i$ ,  $d_i = 2\langle r_i \rangle + e^{j\phi}u_{i+1}$ , and  $f_i = \langle r_i \rangle - e^{j2\phi}u_{i+2}$ . We then denote variable  $v_i$  as in (40), shown at the top of the next page.

2) *Updating  $s_k$* : The variational distribution  $q(s_k)$  is obtained by taking the expectation of the conditional in (32) w.r.t.  $q(\mathbf{r}, \gamma)$ :

$$\begin{aligned} q(s_k) &\propto \exp \left\{ \left\langle \ln p(s_k) + \sum_{i=1}^N \ln p(r_i|r_{i-1}, y_{i-1}, r_{i-2}, y_{i-2}, \mathbf{s}, \gamma; \mathbf{H}) \right\rangle \right\}, \\ &\propto p(s_k) \exp \left\{ -\langle \gamma \rangle \sum_{i=1}^N \left\langle |r_i - \mathbf{h}_i^T \mathbf{s} - 2e^{-j\phi}(r_{i-1} - y_{i-1}) + e^{-j2\phi}(r_{i-2} - y_{i-2})|^2 \right\rangle \right\} \\ &\propto p(s_k) \prod_{i=1}^N \mathcal{CN}(z_{i,k}; h_{i,k}s_k, \langle \gamma \rangle^{-1}), \end{aligned} \quad (41)$$



$$\begin{aligned}
q(r_i) &\propto p(y_i|r_i) \exp \left\{ - \langle \gamma |r_i - \mathbf{h}_i^T \mathbf{s} - 2e^{-j\phi}(r_{i-1} - y_{i-1}) + e^{-j2\phi}(r_{i-2} - y_{i-2})|^2 \rangle - \langle \gamma |r_{i+1} - \mathbf{h}_{i+1}^T \mathbf{s} \right. \\
&\quad \left. - 2e^{-j\phi}(r_i - y_i) + e^{-j2\phi}(r_{i-1} - y_{i-1})|^2 \rangle - \langle \gamma |r_{i+2} - \mathbf{h}_{i+2}^T \mathbf{s} - 2e^{-j\phi}(r_{i+1} - y_{i+1}) + e^{-j2\phi}(r_i - y_i)|^2 \rangle \right\} \\
&\propto p(y_i|r_i) \exp \left\{ - \langle \gamma \rangle \langle |r_i - \mathbf{h}_i^T \mathbf{s} - 2e^{-j\phi}(r_{i-1} - y_{i-1}) + e^{-j2\phi}(r_{i-2} - y_{i-2})|^2 \rangle - \langle \gamma \rangle \langle |2(r_i - y_i) - e^{j\phi}r_{i+1} \right. \\
&\quad \left. + e^{j\phi}\mathbf{h}_{i+1}^T \mathbf{s} - e^{-j\phi}(r_{i-1} - y_{i-1})|^2 \rangle - \langle \gamma \rangle \langle |r_i - y_i + e^{j2\phi}r_{i+2} - e^{j2\phi}\mathbf{h}_{i+2}^T \mathbf{s} - 2e^{j\phi}(r_{i+1} - y_{i+1})|^2 \rangle \right\} \\
&\propto \mathbb{1}(r_i \in [y_i^{\text{low}}, y_i^{\text{up}}]) \exp \left\{ - \langle \gamma \rangle (|r_i - c_i|^2 + |2r_i - d_i|^2 + |r_i - f_i|^2) \right\} \\
&\propto \mathbb{1}(r_i \in [y_i^{\text{low}}, y_i^{\text{up}}]) \exp \left\{ - 6\langle \gamma \rangle |r_i - (c_i + 2d_i + f_i)/6|^2 \right\} \\
&\propto \mathbb{1}(r_i \in [y_i^{\text{low}}, y_i^{\text{up}}]) \mathcal{CN}(r_i; (c_i + 2d_i + f_i)/6, 1/(6\langle \gamma \rangle))
\end{aligned} \tag{36}$$

$$v_i = \begin{cases} \frac{c_i + 2d_i + f_i}{6} = \langle r_i \rangle - \frac{u_i - 2e^{j\phi}u_{i+1} + e^{j2\phi}u_{i+2}}{6} & \text{for } i = 1, \dots, N-2, \\ \frac{c_{N-1} + 2d_{N-1}}{5} = \langle r_{N-1} \rangle - \frac{u_{N-1} - 2e^{j\phi}u_N}{5} & \text{for } i = N-1, \\ c_N = \langle r_N \rangle - u_N & \text{for } i = N. \end{cases} \tag{40}$$

where  $z_{i,k}$  is defined as

$$\begin{aligned}
z_{i,k} &= \langle r_i \rangle - 2e^{-j\phi}(\langle r_{i-1} \rangle - y_{i-1}) + e^{-j2\phi}(\langle r_{i-2} \rangle - y_{i-2}) \\
&\quad - \mathbf{h}_i^T \langle \mathbf{s} \rangle + h_{i,k} \langle s_k \rangle \\
&= u_i - h_{i,k} \langle s_k \rangle.
\end{aligned} \tag{42}$$

The variational mean  $\langle s_k \rangle$  and variance  $\tau_{s_k}$  then can be obtained accordingly.

3) *Updating  $\gamma$* : The variational distribution  $q(\gamma)$  can be obtained by taking the expectation of the conditional distribution in (32) w.r.t.  $q(\mathbf{s}, \mathbf{r})$  as

$$\begin{aligned}
q(\gamma) &\propto \exp \left\{ \left\langle \ln p(\gamma) \right. \right. \\
&\quad \left. \left. + \sum_{i=1}^N \ln p(r_i | r_{i-1}, y_{i-1}, r_{i-2}, y_{i-2}, \mathbf{s}, \gamma; \mathbf{H}) \right\rangle \right\}, \tag{43}
\end{aligned}$$

which is expanded as in (44) on the next page, where  $u_i$  denotes the residual term at receive antenna  $i$ . The variational distribution  $q(\gamma)$  is Gamma with mean

$$\langle \gamma \rangle = \frac{N + \alpha}{\beta + \|\mathbf{u}\|^2 + 6\text{Tr}\{\mathbf{\Sigma}_r\} - 5\tau_{r_N} - \tau_{r_{N-1}} + \text{Tr}\{\mathbf{H}\mathbf{\Sigma}_s\mathbf{H}^H\}}. \tag{45}$$

The proposed VB method for MIMO detection with 2<sup>nd</sup>-order  $\Sigma\Delta$  quantization is summarized in Algorithm 2, where the parameter  $\epsilon$  is the numerator of  $\hat{\gamma}$  in the variational distributions of (35), (37), and (38) for updating  $r_i$ ,  $r_{N-1}$ , and  $r_N$ , respectively.

### B. Computational Complexity Analysis

The computational complexity of the proposed algorithms is analyzed here assuming  $N \geq K$ . For iterative algorithms, the complexity order is given per iteration. For LMMSE, the computation of  $\mathbf{H}\mathbf{\Sigma}_s\mathbf{H}^H$  for the linear detector in (13) requires a complexity of  $\mathcal{O}(NK^2)$ , while calculating  $\mathbf{U}^{-1}\mathbf{\Sigma}_q\mathbf{U}^{-H}$  requires  $\mathcal{O}(N^3)$  operations due to the matrix inversion. In addition, the denoiser for  $K$  users contributes a complexity of  $\mathcal{O}(|S|K)$ . Thus, the overall computational burden of the

### Algorithm 2 – VB Algorithm for MIMO Detection with 2<sup>nd</sup>-Order $\Sigma\Delta$ Quantization

---

```

1: Input:  $\mathbf{y}, \mathbf{H}$ 
2: Output:  $\hat{\mathbf{s}}$ 
3: Initialize  $\hat{r}_i^1 = y_i^1$ ,  $\tau_{r_i}^1 = 0$ ,  $\forall i$ ,  $\hat{s}_k^1 = 0$ ,  $\tau_{s_k}^1 = \text{Var}_{p(s_k)}[s_k]$ ,  $\forall k$ ,
 $\mathbf{u} = \hat{\mathbf{r}}^1 - \mathbf{H}\hat{\mathbf{s}}^1$ .
4: for  $t = 1, 2, \dots$  do
5:    $\hat{\gamma}^t \leftarrow (N + \alpha) / (\beta + \|\mathbf{u}\|^2 + 6\text{Tr}\{\mathbf{\Sigma}_r\} - 5\tau_{r_N}^t - \tau_{r_{N-1}}^t$ 
6:      $+ \text{Tr}\{\mathbf{H}\mathbf{\Sigma}_s\mathbf{H}^H\})$ 
7:   for  $i = 1, \dots, N$  do
8:     if  $i = N$  then
9:        $v_N^t \leftarrow \hat{r}_N^t - u_N$ ,  $\epsilon = 1$ 
10:    else if  $i = N-1$  then
11:       $v_{N-1}^t \leftarrow \hat{r}_{N-1}^t - (u_{N-1} - 2e^{j\phi}u_N)/2$ ,  $\epsilon = 5$ 
12:    else
13:       $v_i^t \leftarrow \hat{r}_i^t - (u_i - 2e^{j\phi}u_{i+1} + e^{j2\phi}u_{i+2})/6$ ,  $\epsilon = 6$ 
14:    end if
15:     $\hat{r}_i^{t+1} \leftarrow F_r(v_i^t, \epsilon\hat{\gamma}^t, y_i^{\text{low}}, y_i^{\text{up}})$ 
16:     $\tau_{r_i}^{t+1} \leftarrow G_r(v_i^t, \epsilon\hat{\gamma}^t, y_i^{\text{low}}, y_i^{\text{up}})$ 
17:     $u_i \leftarrow u_i - \hat{r}_i^t + \hat{r}_i^{t+1}$ 
18:     $u_{i+1} \leftarrow u_{i+1} + 2e^{-j\phi}(\hat{r}_i^t - \hat{r}_i^{t+1})$  only for  $i < N$ 
19:     $u_{i+2} \leftarrow u_{i+2} - e^{-j2\phi}(\hat{r}_i^t - \hat{r}_i^{t+1})$  only for  $i < N-1$ 
20:  end for
21:  for  $k = 1, \dots, K$  do
22:     $\mathbf{z}_k^t \leftarrow \mathbf{h}_k \hat{s}_k^t + \mathbf{u}$ 
23:     $\hat{s}_k^{t+1} \leftarrow F_s(\mathbf{z}_k^t, \mathbf{h}_k, \hat{\gamma}^t)$ 
24:     $\tau_{s_k}^{t+1} \leftarrow G_s(\mathbf{z}_k^t, \mathbf{h}_k, \hat{\gamma}^t)$ 
25:     $\mathbf{u} \leftarrow \mathbf{u} + \mathbf{h}_k(\hat{s}_k^t - \hat{s}_k^{t+1})$ 
26:  end for
27: end for
28:  $\forall k : \hat{s}_k \leftarrow \arg \max_{a \in S} p_a \mathcal{CN}(\mathbf{z}_k^t; \mathbf{h}_k a, (1/\hat{\gamma}^t)\mathbf{I}_M)$ 

```

---

LMMSE detector is dominated by the matrix inversion, resulting in an overall complexity of order  $\mathcal{O}(N^3 + |S|K)$ . For the 1<sup>st</sup>- and 2<sup>nd</sup>-order SD-VB algorithms in Algs. 1 and 2, respectively, the cost to compute  $\text{Tr}\{\mathbf{H}\mathbf{\Sigma}_s\mathbf{H}^H\} = \sum_{k=1}^K \tau_{s_k} \|\mathbf{h}_k\|^2$  in step 5 is  $\mathcal{O}(NK)$ , which dominates that for computing the residual vector  $\|\mathbf{u}\|^2$  which is  $\mathcal{O}(N)$ . The computation in step 18 of Algorithm 1 and step 22 of Algorithm 2 adds a complexity of  $\mathcal{O}(|S|)$  for each user. The overall per-iteration complexity of Algs. 1 and 2 is thus  $\mathcal{O}(NK + |S|K)$ , and we see that the 1<sup>st</sup>- and 2<sup>nd</sup>-order SD-VB algorithms have the



$$\begin{aligned}
q(\gamma) &\propto \exp \left\{ (N + \alpha - 1) \ln \gamma - \beta \gamma - \gamma \sum_{i=1}^N \left\langle |r_i - \mathbf{h}_i^T \mathbf{s} - 2e^{-j\phi}(r_{i-1} - y_{i-1}) + e^{-j2\phi}(r_{i-2} - y_{i-2})|^2 \right\rangle \right\} \\
&\propto \exp \left\{ (N + \alpha - 1) \ln \gamma - \beta \gamma - \gamma \sum_{i=1}^N [ |u_i|^2 + \tau_{r_i} + \mathbf{h}_i^H \boldsymbol{\Sigma}_s \mathbf{h}_i + 4\tau_{r_{i-1}} + \tau_{r_{i-2}} ] \right\} \\
&\propto \exp \left\{ (N + \alpha - 1) \ln \gamma - \gamma(\beta + \|\mathbf{u}\|^2 + 6\text{Tr}\{\boldsymbol{\Sigma}_r\} + \text{Tr}\{\mathbf{H}\boldsymbol{\Sigma}_s\mathbf{H}^H\} - 5\tau_{r_N} - \tau_{r_{N-1}}) \right\}, \tag{44}
\end{aligned}$$

TABLE I: Algorithm Computational Complexity

Algorithm	Complexity
MF-VB in [28]	$\mathcal{O}(NKT +  S KT)$
MF-QVB in [10]	$\mathcal{O}(NKT +  S KT)$
LMMSE	$\mathcal{O}(N^3 +  S K)$
1 <sup>st</sup> -order SD-VB	$\mathcal{O}(NKT +  S KT)$
2 <sup>nd</sup> -order SD-VB	$\mathcal{O}(NKT +  S KT)$

same complexity as that for the MF-VB and MF-QVB approaches, although the  $\Sigma\Delta$  methods can provide a significant improvement in MIMO detection performance under the given assumptions of spatial oversampling or sectored users. Note that the complexities of the VB-based algorithms presented in Table I also indicate the number of iterations  $T$  required for convergence. Our simulations indicate that  $T$  is typically less than 10.

## VI. NUMERICAL RESULTS

In this section, we present illustrative numerical results for the performance of the proposed 1<sup>st</sup>- and 2<sup>nd</sup>-order SD-VB algorithms compared with state-of-the-art data detection methods such as the matched-filter quantized VB (MF-QVB) in [10] and LMMSE-based detection for various scenarios. We implement all VB-based algorithms with a maximum of 50 iterations and consider scenarios with 100 transmitted data symbols. The noise variance  $N_0$  is set based on the SNR, which is defined as

$$\text{SNR} = \frac{\mathbb{E}[\|\mathbf{H}\mathbf{s}\|^2]}{\mathbb{E}[\|\mathbf{n}\|^2]} = \frac{K}{NN_0}. \tag{46}$$

Unless otherwise stated, all cases assume the number of paths as  $L = 20$ , the width of the angular sector as  $\Theta = 40^\circ$  and assume it is centered at  $\theta_0 = 0^\circ$ . We assume all users lie within the same azimuth angular range, with AoAs drawn uniformly from the interval  $[-20^\circ, 20^\circ]$ . We also assume the number of BS antennas is  $N = 128$ , the number of users is  $K = 16$ , the phase shift of the  $\Sigma\Delta$  array is  $\phi = 2\pi \frac{d}{\lambda} \sin(\theta_0)$ ,  $d = \lambda/6$ , and the users employ QPSK signaling.

To highlight the effectiveness of the proposed approach, we compare the performance of the SD-VB algorithms with that of the following benchmark approaches:

- 1) The LMMSE receiver presented in Section III implemented with the 1<sup>st</sup>-order  $\Sigma\Delta$  architecture and 1-bit quantizers,
- 2) The MF-QVB algorithm developed in [10] implemented with conventional few-bit quantizers,

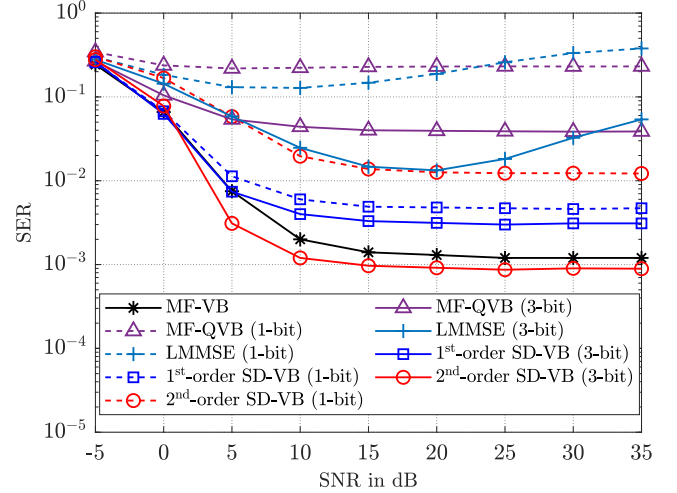


Fig. 5: SER performance of various algorithms vs. SNR with 1-bit and 3-bit quantizers,  $\theta_0 = 20^\circ$ ,  $\Theta = 40^\circ$ , and  $d = \lambda/6$ .

- 3) The MF-VB algorithm developed in [28] implemented with ideal/infinite quantizers.

Fig. 5 shows the data detection performance improvement of the algorithms using 1-bit and 3-bit quantization. The SD-VB algorithms outperform MF-QVB since the  $\Sigma\Delta$  receivers shape the quantization noise away from the spatial frequencies of interest. The SD-VB algorithms also significantly outperform the LMMSE-based receiver because the latter's reliance on linear processing makes it ineffective at separating users with highly correlated channels. We note that the SERs of all algorithms that process quantized signals converge to their error floors at high SNR because the quantization noise becomes the dominant source of error.

The performance of 2<sup>nd</sup>-order SD-VB significantly improves when the ADC resolution is increased from 1 to 3 bits, achieving the best SER among the considered algorithms, while MF-QVB performs the worst. This advantage is due to the more aggressive noise shaping of the 2<sup>nd</sup>-order  $\Sigma\Delta$  architecture, greatly reducing the quantization noise in lower spatial frequency ranges. Although MF-QVB shows some improvement with 3-bit quantization, it remains inefficient for cases with users confined to an angular sector since the quantization noise is uniformly spread across all spatial frequencies. While the MF-VB algorithm employs ideal/infinite quantization, it also experiences an error floor due to the channel correlation [28]. The 2<sup>nd</sup>-order SD-VB with only 3-bit quantizers outperforms MF-VB since it implicitly exploits knowledge of the

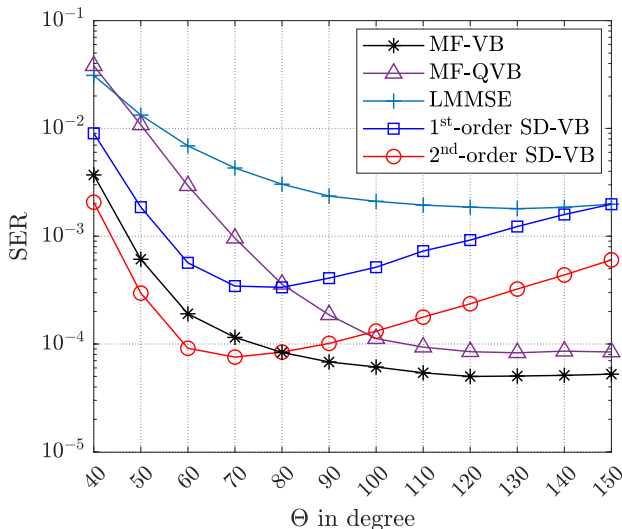


Fig. 6: SER performance vs. azimuth angular spread  $\Theta$ , with 3-bit quantizers, SNR = 5 dB,  $\theta_0 = 0^\circ$ , and  $d = \lambda/6$ .

angular sector to which the users are confined and the resulting spatial correlation. While LMMSE receiver provided in (13) is designed for 1-bit quantization, it shows considerable SER improvement when the quantization resolution is increased to 3 bits. Thus, in subsequent simulations we will only show results for the 3-bit LMMSE implementation.

Fig. 6 shows the effect of the azimuth angular spread on SER performance. For narrow azimuth ranges, all approaches experience high SER due to the extreme channel correlation that results in  $K = 16$  users densely packed together. The 3-bit SD-VB implementation has the best performance among all the approaches for sectors smaller than  $80^\circ$ . Both SD-VB implementations achieve their best performance for  $\Theta \in [60^\circ, 80^\circ]$ , but their SERs degrade as the sectors become wider since the noise-shaping effect is limited. MF-VB and MV-QVB have the best performance for large sectors since the  $\Sigma\Delta$ -based approaches have reduced spatial correlation to exploit. The advantage of using VB, in general, is evident in the superior performance of the VB algorithms compared with LMMSE in all cases.

Fig. 7 presents the effect of antenna spacing and wavelength on the SER performance of all detection algorithms for an array with a fixed number of antennas ( $N = 128$ ). Observations similar to those in the previous example can be made here. In particular, when  $d$  is very small, the array aperture is significantly reduced and none of the methods are able to counteract the extreme channel correlation that results from the narrow angular sector of  $\Theta = 40^\circ$ . The SER of all algorithms improves with increasing  $d$ , although the 1<sup>st</sup>- and 2<sup>nd</sup>-order SD-VB algorithms provide the best performance for values of  $d$  around  $1/4$  to  $1/3$ , and degrade for larger  $d$  since the benefit of oversampling is lost. As the antenna spacing increases, the reduced channel correlation benefits MF-VB and MF-QVB.

In Fig. 8 we also study the impact of the antenna spacing  $d$ , but in this case we fix the array aperture  $d_0 = Nd$  so that as  $d$  decreases, the number of antennas  $N$  increases. For

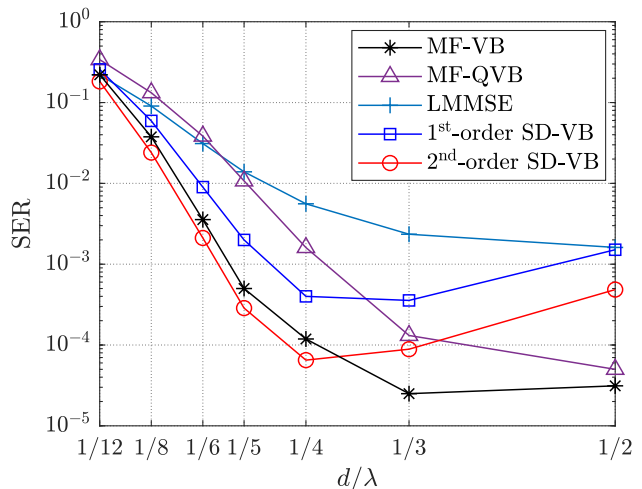


Fig. 7: SER performance vs.  $d/\lambda$ , with 3-bit quantizers,  $N = 128$ ,  $\Theta = 40^\circ$ ,  $\theta_0 = 0^\circ$ , and SNR = 5 dB.

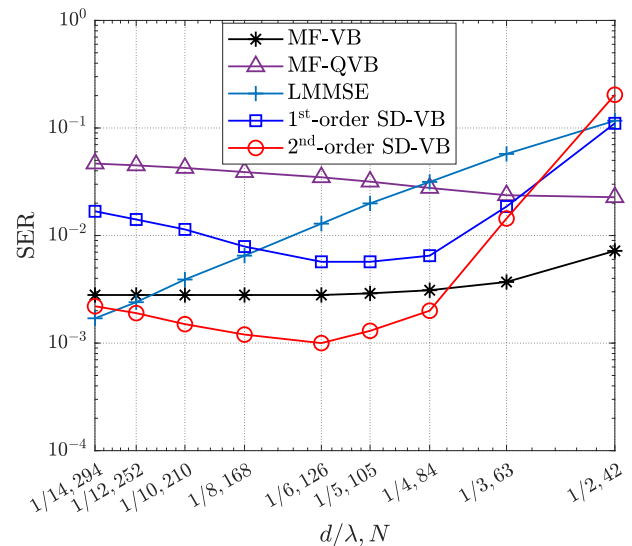


Fig. 8: SER performance vs.  $(d/\lambda, N)$ , with a fixed array  $d_0 = 14$  cm, 3-bit quantizers,  $K = 16$ ,  $\Theta = 40^\circ$ ,  $\theta_0 = 0^\circ$ , and SNR = 8 dB.

example, if the aperture is set at  $d_0 = Nd = 14$  cm, the wavelength is  $\lambda = c/f = 6.7$  mm at  $f = 45$  GHz, and as  $d$  decreases from  $\lambda/2$  to  $\lambda/14$ ,  $N$  increases from 42 to 294. As shown in the figure, in this case there is much less degradation for small  $d$  since the larger array aperture maintains a more constant level of channel correlation. Interestingly, the LMMSE receiver benefits the most from the increase in  $N$ , and yields better performance than the MF-VB and SD-VB for very small  $d$ . In this case, the best trade-off between the number of observations and the channel correlation for the SD-VB algorithms occurs for  $d = \lambda/6$ . It is critical to note that the two previous examples have ignored the impact of mutual coupling, which will become important as  $d$  becomes much smaller than  $\lambda/2$ . Interestingly, as shown in [41], the  $\Sigma\Delta$  approach benefits to some extent from mutual coupling due to the increase in correlation between the signals at adjacent

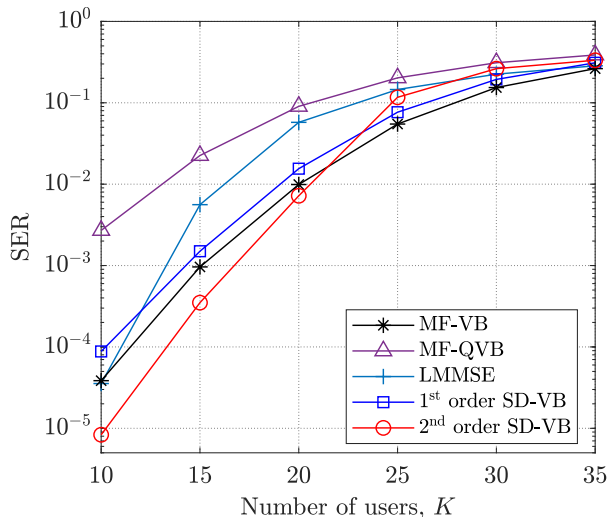


Fig. 9: SER performance vs. number of users with 3-bit quantizers, SNR = 8 dB,  $N = 80$ ,  $d = \lambda/6$ ,  $\theta_0 = 0^\circ$ , and  $\Theta = 40^\circ$ .

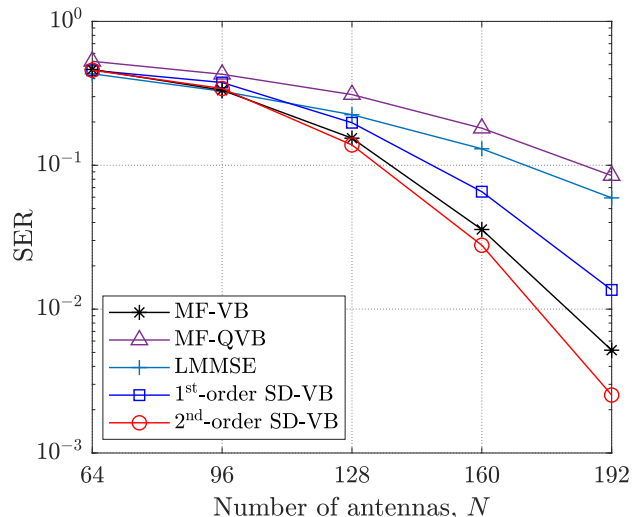


Fig. 10: SER performance vs. number of antennas with 3-bit quantizers, SNR = 8 dB,  $K = 30$ ,  $d = \lambda/6$ ,  $\theta_0 = 0^\circ$ , and  $\Theta = 40^\circ$ .

antennas. This is an issue that requires further study for the VB-based algorithms.

In Fig. 9, we show the effects of the number of users  $K$  on the detection performance. When  $K$  decreases, the lower spatial channel correlation enhances the data detection performance of all algorithms. The 2<sup>nd</sup>-order SD-VB algorithm achieves the lowest SER among the considered algorithms when  $K \leq 10$ , including MF-VB with infinite precision ADCs. On the other hand, MF-VB has the best performance for large  $K$ , but in these cases the SER is already quite high. MF-QVB performs the worst due to its use of matched filtering to handle multiuser interference, which is suboptimal with high channel correlation, even with relatively few users. LMMSE excels with a small number of users since it is able to more effectively eliminate inter-user interference, achieving a lower SER than MF-VB, 1<sup>st</sup>-order SD-VB, and MF-QVB when  $K = 10$ .

In Fig. 10 we present results for data detection with different numbers of antennas. As  $N$  increases, the 1<sup>st</sup>- and 2<sup>nd</sup>-order SD-VB algorithms show significant SER improvement, while the improvement is marginal for LMMSE and MF-QVB. Moreover, the SER performance gap between 2<sup>nd</sup>-order SD-VB and the other detection algorithms becomes wider as the number of antennas increases.

Fig. 11 displays the SER for the  $\Sigma\Delta$  algorithms as a function of the ADC resolution  $b$  for  $d = \lambda/8$  and  $d = \lambda/6$ . While the SER decreases as  $b$  increases to 3, there is relatively little improvement for higher ADC resolutions. The 1<sup>st</sup>-order SD-VB approach offers better data detection performance than 2<sup>nd</sup>-order SD-VB for 1-bit quantization. This can occur when the 1-bit ADCs in a 2<sup>nd</sup>-order  $\Sigma\Delta$  architecture becomes overloaded, a condition that occurs when where the input signals combined with the quantization noise exceed the full-scale range of the 1-bit quantizer leading to instability [19].

Fig. 12 shows the SER of the LMMSE, 1<sup>st</sup>-order SD-VB, and 2<sup>nd</sup>-order SD-VB algorithms for 3-bit  $\Sigma\Delta$  architectures

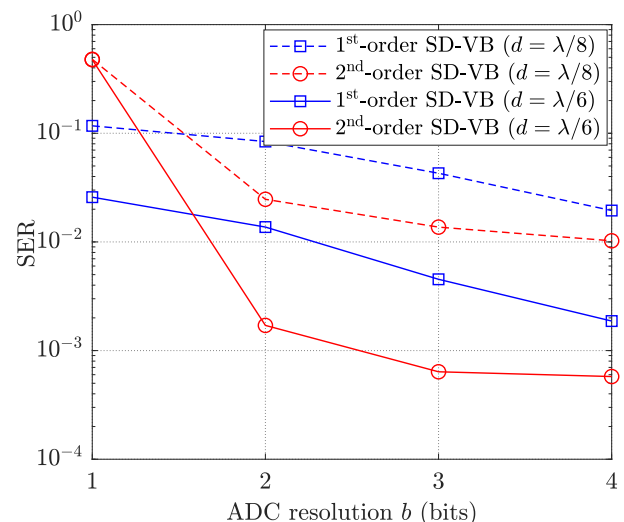


Fig. 11: SER performance vs.  $\Sigma\Delta$  ADC resolution  $b$  bits with SNR = 12 dB,  $\theta_0 = 0$ ,  $d = \lambda/6$ , and  $\Theta = 40^\circ$ .

implemented with different steering angles  $\phi = 2\pi \frac{d}{\lambda} \sin(\theta)$ . The steering angles are varied while the center angle of the sector is set as  $\theta_0 = 0^\circ, 30^\circ$ , and  $60^\circ$  in Figs. 12(a), 12(b), and 12(c), respectively. Results for MF-VB are included as a reference, although its performance does not depend on  $\phi$  since it does not use the  $\Sigma\Delta$  implementation. As expected, the lowest SER for the 1<sup>st</sup>- and 2<sup>nd</sup>-order SD-VB architectures is obtained when the steering angle is chosen to match the center angle of the sector, i.e.,  $\theta = \theta_0$ . The SER performance of all algorithms degrades as the center angle of the sector increases, since the ability of the array to spatially separate the signals decreases. LMMSE performs best without a phase offset, and degrades significantly as the angular sector of the users moves away from broadside.

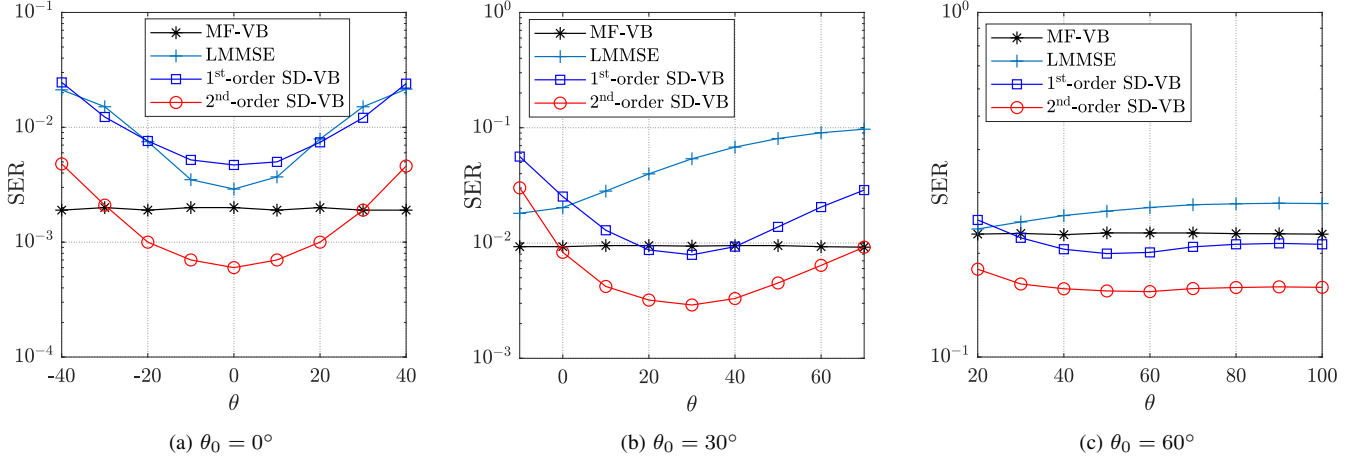


Fig. 12: SER performance vs. different steering angles  $\phi = 2\pi \frac{d}{\lambda} \sin(\theta)$  of  $\Sigma\Delta$  ADCs with 3-bit quantizers, SNR= 12 dB and  $d = \lambda/6$ .

## VII. CONCLUSIONS

In this paper, we have developed two MIMO detection algorithms based on the VB inference framework in massive MIMO systems with few-bit  $\Sigma\Delta$  ADCs. We first modeled the Bayesian networks for the 1<sup>st</sup>- and 2<sup>nd</sup>-order  $\Sigma\Delta$  receivers, based on which the variational distributions of the latent variables were obtained in closed form. We then proposed two iterative algorithms for MIMO detection with efficient updates and low-complexity implementation. Simulation results showed that the proposed 1<sup>st</sup>- and 2<sup>nd</sup>-order SD-VB algorithms achieve their best data detection performance when the users are confined to angular sectors less than  $80^\circ$  wide and with antenna spacings on the order of  $1/4$  to  $1/6$  a wavelength. Under these conditions, a 2<sup>nd</sup>-order SD-VB approach with 3-bit ADCs can outperform the MF-VB algorithm implemented with infinite resolution quantization, since SD-VB directly exploits the users' spatial correlation. The simulation results also suggest using 1<sup>st</sup>-order SD-VB rather than the 2<sup>nd</sup>-order SD-VB implementation with 1-bit quantization due to potential ADC overloading and unstable performance.

### APPENDIX A

#### CALCULATION OF $F_r(\mu, \gamma, a, b)$ AND $G_r(\mu, \gamma, a, b)$

Define  $\alpha = \sqrt{2\gamma}(a - \mu)$  and  $\beta = \sqrt{2\gamma}(b - \mu)$ . For an arbitrary complex random variable  $\mathcal{CN}(\mu, \gamma^{-1})$  whose real and imaginary parts are both truncated on the interval  $(a, b)$ , the mean  $F_r(\mu, \gamma, a, b)$  and variance  $G_r(\mu, \gamma, a, b)$  are given by [10]

$$F_r(\mu, \gamma, a, b) = \mu - \frac{1}{\sqrt{2\gamma}} \frac{f(\beta) - f(\alpha)}{F(\beta) - F(\alpha)}, \quad (47)$$

$$G_r(\mu, \gamma, a, b) = \frac{1}{2\gamma} \left[ 1 - \frac{\beta f(\beta) - \alpha f(\alpha)}{F(\beta) - F(\alpha)} - \left( \frac{f(\beta) - f(\alpha)}{F(\beta) - F(\alpha)} \right)^2 \right], \quad (48)$$

where  $f(x)$  and  $F(x)$  denote the PDF and CDF of a standard Gaussian random variable, respectively.

For the case of 1-bit quantizers, the three quantization thresholds are:  $\{-\infty, 0, \infty\}$ , simplifying the computation of

$F_r(\mu, \gamma, a, b)$  and  $G_r(\mu, \gamma, a, b)$ . Denoting  $\zeta = \text{sign}(y)\sqrt{2\gamma}\mu$  with quantization level  $y$ , we have

$$F_r(\mu, \gamma, a, b) = \mu + \frac{\text{sign}(y)}{\sqrt{2\gamma}} \frac{f(\zeta)}{F(\zeta)},$$

$$G_r(\mu, \gamma, a, b) = \frac{1}{2\gamma} \left[ 1 - \frac{\zeta f(\zeta)}{F(\zeta)} - \left( \frac{f(\zeta)}{F(\zeta)} \right)^2 \right].$$

### APPENDIX B

#### CALCULATION OF $F_s(\mathbf{z}_k, \mathbf{h}_k, \gamma)$ AND $G_s(\mathbf{z}_k, \mathbf{h}_k, \gamma)$

Given  $\mathbf{z}_k = \mathbf{h}_k s_k + \mathcal{CN}(\mathbf{0}, \gamma^{-1} \mathbf{I}_N)$ , the posterior distribution of  $s_k$  given  $\mathbf{z}_k$  is

$$p(s_k | \mathbf{z}_k; \mathbf{h}_k, \gamma) \propto p(s_k) \prod_{i=1}^N \mathcal{CN}(z_{i,k}; h_{i,k} s_k, \gamma^{-1}). \quad (49)$$

For  $a \in \mathcal{S}$ , we have

$$p(s_k = a | \mathbf{z}_k; \mathbf{h}_k, \gamma) = \frac{p_a}{Z} \exp \left\{ -\gamma \sum_{i=1}^N |z_{i,k} - h_{i,k} a|^2 \right\}, \quad (50)$$

where  $Z = \sum_{b \in \mathcal{S}} p_b \exp \left\{ -\gamma \sum_{i=1}^N |z_{i,k} - h_{i,k} b|^2 \right\}$ . The variational mean and variance of the posterior distribution in (49) can be calculated as

$$F_s(\mathbf{z}_k, \mathbf{h}_k, \gamma) = \sum_{a \in \mathcal{S}} a p(s_k = a | \mathbf{z}_k; \mathbf{h}_k, \gamma), \quad (51)$$

$$G_s(\mathbf{z}_k, \mathbf{h}_k, \gamma) = \sum_{a \in \mathcal{S}} |a|^2 p(s_k = a | \mathbf{z}_k; \mathbf{h}_k, \gamma) - |F_s(\mathbf{z}_k, \mathbf{h}_k, \gamma)|^2. \quad (52)$$

### REFERENCES

- [1] T.-V. Nguyen, S. Nassirpour, I. Atzeni, A. Töllli, A. L. Swindlehurst, and D. H. N. Nguyen, "Optimal detection in MIMO systems using spatial sigma-delta ADCs," in *Proc. 58th Asilomar Conf. on Signals, Systems, and Computers*, Oct. 2024.
- [2] N. Rajatheva, I. Atzeni, E. Bjornson, A. Bourdoux, S. Buzzi, J.-B. Dore, S. Erkucuk, M. Fuentes, K. Guan, Y. Hu *et al.*, "White paper on broadband connectivity in 6G," *arXiv preprint arXiv:2004.14247*, 2020.

- [3] D. H. N. Nguyen, L. B. Le, T. Le-Ngoc, and R. W. Heath, "Hybrid MMSE precoding and combining designs for mmwave multiuser systems," *IEEE Access*, vol. 5, pp. 19 167–19 181, 2017.
- [4] S. Buzzi and C. D'Andrea, "Energy efficiency and asymptotic performance evaluation of beamforming structures in doubly massive MIMO mmWave systems," *IEEE Trans. Green Commun. Netw.*, vol. 2, no. 2, pp. 385–396, 2018.
- [5] F. Sohrabi, Y.-F. Liu, and W. Yu, "One-bit precoding and constellation range design for massive MIMO with QAM signaling," *IEEE J. Sel. Top. Signal Process.*, vol. 12, no. 3, pp. 557–570, 2018.
- [6] H. Jedda, A. Mezghani, A. L. Swindlehurst, and J. A. Nossek, "Quantized constant envelope precoding with PSK and QAM signaling," *IEEE Trans. Wireless Commun.*, vol. 17, no. 12, pp. 8022–8034, 2018.
- [7] B. Fesl, M. Koller, and W. Utschick, "On the mean square error optimal estimator in one-bit quantized systems," *IEEE Trans. Signal Process.*, vol. 71, pp. 1968–1980, 2023.
- [8] K. Roth, H. Pirzadeh, A. L. Swindlehurst, and J. A. Nossek, "A comparison of hybrid beamforming and digital beamforming with low-resolution ADCs for multiple users and imperfect CSI," *IEEE J. Sel. Top. Signal Process.*, vol. 12, no. 3, pp. 484–498, 2018.
- [9] K. Safa, R. Combes, R. De Lacerda, and S. Yang, "Data detection in 1-bit quantized MIMO systems," *IEEE Trans. Commun. (Early Access)*, Apr. 2024.
- [10] L. V. Nguyen, A. L. Swindlehurst, and D. H. N. Nguyen, "Variational Bayes for joint channel estimation and data detection in few-bit massive MIMO systems," *IEEE Trans. Signal Process.*, 2024.
- [11] Y. Li, C. Tao, G. Seco-Granados, A. Mezghani, A. L. Swindlehurst, and L. Liu, "Channel estimation and performance analysis of one-bit massive MIMO systems," *IEEE Trans. Signal Process.*, vol. 65, no. 15, pp. 4075–4089, 2017.
- [12] J. Zhang, L. Dai, S. Sun, and Z. Wang, "On the spectral efficiency of massive MIMO systems with low-resolution ADCs," *IEEE Commun. Lett.*, vol. 20, no. 5, pp. 842–845, 2016.
- [13] L. Fan, S. Jin, C.-K. Wen, and H. Zhang, "Uplink achievable rate for massive MIMO systems with low-resolution ADC," *IEEE Commun. Lett.*, vol. 19, no. 12, pp. 2186–2189, 2015.
- [14] A. K. Saxena, I. Fijalkow, and A. L. Swindlehurst, "Analysis of one-bit quantized precoding for the multiuser massive MIMO downlink," *IEEE Trans. Signal Process.*, vol. 65, no. 17, pp. 4624–4634, 2017.
- [15] A. Bazrafkan and N. Zlatanov, "Asymptotic capacity of massive MIMO with 1-bit ADCs and 1-bit DACs at the receiver and at the transmitter," *IEEE Access*, vol. 8, pp. 152 837–152 850, 2020.
- [16] L. V. Nguyen, A. L. Swindlehurst, and D. H. N. Nguyen, "SVM-based channel estimation and data detection for one-bit massive MIMO systems," *IEEE Trans. Signal Process.*, vol. 69, pp. 2086–2099, 2021.
- [17] J. M. de la Rosa, "Sigma-delta modulators: Tutorial overview, design guide, and state-of-the-art survey," *IEEE Trans. Circuits Syst. I: Regul. Pap.*, vol. 58, no. 1, pp. 1–21, 2010.
- [18] S. Rao, G. Seco-Granados, H. Pirzadeh, J. A. Nossek, and A. L. Swindlehurst, "Massive MIMO channel estimation with low-resolution spatial sigma-delta ADCs," *IEEE Access*, vol. 9, pp. 109 320–109 334, 2021.
- [19] P. M. Aziz, H. V. Sorensen, and J. Van der Spiegel, "An overview of sigma-delta converters," *IEEE Signal Process. Mag.*, vol. 13, no. 1, pp. 61–84, 1996.
- [20] H. Pirzadeh, G. Seco-Granados, S. Rao, and A. L. Swindlehurst, "Spectral efficiency of one-bit sigma-delta massive MIMO," *IEEE J. Sel. Areas Commun.*, vol. 38, no. 9, pp. 2215–2226, 2020.
- [21] R. P. Sankar and S. P. Chepuri, "Channel estimation in MIMO systems with one-bit spatial sigma-delta ADCs," *IEEE Trans. Signal Process.*, vol. 70, pp. 4681–4696, 2022.
- [22] I. Atzeni, A. Tölli, D. H. N. Nguyen, and A. L. Swindlehurst, "Doubly 1-bit quantized massive MIMO," *arXiv preprint arXiv:2312.01777*, 2023.
- [23] Y.-S. Jeon, N. Lee, S.-N. Hong, and R. W. Heath, "One-bit sphere decoding for uplink massive MIMO systems with one-bit ADCs," *IEEE Trans. Wireless Commun.*, vol. 17, no. 7, pp. 4509–4521, 2018.
- [24] Y.-S. Jeon, N. Lee, and H. V. Poor, "Robust data detection for MIMO systems with one-bit ADCs: A reinforcement learning approach," *IEEE Trans. Wireless Commun.*, vol. 19, no. 3, pp. 1663–1676, 2019.
- [25] L. V. Nguyen, D. H. Nguyen, and A. L. Swindlehurst, "SVM-based channel estimation and data detection for massive MIMO systems with one-bit ADCs," in *Proc. IEEE Int'l Conf. on Communications (ICC)*, 2020.
- [26] Y.-S. Jeon, S.-N. Hong, and N. Lee, "Supervised-learning-aided communication framework for MIMO systems with low-resolution ADCs," *IEEE Trans. Veh. Technol.*, vol. 67, no. 8, pp. 7299–7313, 2018.
- [27] S. Khobahi, N. Shlezinger, M. Soltanalian, and Y. C. Eldar, "LoRD-Net: Unfolded deep detection network with low-resolution receivers," *IEEE Trans. Signal Process.*, vol. 69, pp. 5651–5664, 2021.
- [28] D. H. N. Nguyen, I. Atzeni, A. Tölli, and A. L. Swindlehurst, "A variational Bayesian perspective on massive MIMO detection," *arXiv preprint arXiv:2205.11649*, 2022.
- [29] S. S. Thoota and C. R. Murthy, "Variational Bayes joint channel estimation and soft symbol decoding for uplink massive MIMO systems with low resolution ADCs," *IEEE Trans. Commun.*, vol. 69, no. 5, pp. 3467–3481, 2021.
- [30] Y. Xiang, K. Xu, B. Xia, and X. Cheng, "Bayesian joint channel-and-data estimation for quantized OFDM over doubly selective channels," *IEEE Trans. Wireless Commun.*, vol. 22, no. 3, pp. 1523–1536, 2022.
- [31] D. S. Palguna, D. J. Love, T. A. Thomas, and A. Ghosh, "Millimeter wave receiver design using low precision quantization and parallel  $\Delta\Sigma$  architecture," *IEEE Trans. Wireless Commun.*, vol. 15, no. 10, pp. 6556–6569, 2016.
- [32] M. Shao, W.-K. Ma, Q. Li, and A. L. Swindlehurst, "One-bit sigma-delta MIMO precoding," *IEEE J. Sel. Top. Signal Process.*, vol. 13, no. 5, pp. 1046–1061, 2019.
- [33] R. M. Corey and A. C. Singer, "Spatial sigma-delta signal acquisition for wideband beamforming arrays," in *Proc. 20th Int. ITG Workshop on Smart Antennas (WSA)*, 2016.
- [34] W.-Y. Keung, H. V. Cheng, and W.-K. Ma, "Transmitting data through reconfigurable intelligent surface: A spatial sigma-delta modulation approach," in *Proc. IEEE Int'l Conf. on Acoustics, Speech and Sig. Proc. (ICASSP)*, 2024, pp. 9251–9255.
- [35] J. D. Krieger, C.-P. Yeang, and G. W. Wornell, "Dense delta-sigma phased arrays," *IEEE Trans. Antennas Propag.*, vol. 61, no. 4, pp. 1825–1837, 2013.
- [36] L. V. Nguyen, D. H. Nguyen, and A. L. Swindlehurst, "Deep learning for estimation and pilot signal design in few-bit massive MIMO systems," *IEEE Trans. Wireless Commun.*, vol. 22, no. 1, pp. 379–392, 2022.
- [37] A. Alkhateeb, O. El Ayach, G. Leus, and R. W. Heath, "Channel estimation and hybrid precoding for millimeter wave cellular systems," *IEEE J. Sel. Top. Signal Process.*, vol. 8, no. 5, pp. 831–846, 2014.
- [38] J. J. Bussgang, "Crosscorrelation functions of amplitude-distorted gaussian signals," vol. 216, 1952.
- [39] C. M. Bishop and N. M. Nasrabadi, *Pattern Recognition and Machine Learning*. Springer, 2006, vol. 4, no. 4.
- [40] M. W. et al, "Graphical Models, Exponential Families, and Variational Inference," *Foundations and Trends® in Machine Learning*, vol. 1, no. 1–2, pp. 1–305, 2008.
- [41] H. Pirzadeh, G. Seco-Granados, A. L. Swindlehurst, and J. A. Nossek, "On the effect of mutual coupling in one-bit spatial sigma-delta massive MIMO systems," in *Proc. 21st IEEE International Workshop on Signal Processing Advances in Wireless Communications (SPAWC)*, 2020.